Heavy Silylchalcogenido Lanthanates $Ph_4P[Cp_3La\text{-}ESiMe_3]$ (E = S, Se, Te) via Fluoride-Induced Demethylation of Dimethylcarbonate to $Ph_4P[OCO_2Me]$ Key Intermediate

Jannick Guschlbauer, Tobias Vollgraff, Xiulan Xie, Ahmed Fetoh, Jörg Sundermeyer*

Supporting Information

Content

1. Additional experiments

As no suitable single crystals of **2** could be grown for XRD structure determination, we applied the reaction route to other organic fluoride salts (or ion pairs), like the PPN[F] (**2-PPN**), $[Me_3P{=}N{=}P(NMe_2)_3]F$ (**2-PPNMe$_2$**) and TBA[F] · 3 H_2O (**1-TBA**). In PPN[F] (**1-PPN**), the fluoride ion is known to be loosely coordinated to both phosphorous atoms.[1] $[Me_3P{=}N{=}P(NMe_2)_3]F$ and [PPN]F were prepared by a literature-known procedure reacting $[Me_3P{=}N{=}P(NMe_2)_3]BF_4$[2] or $[PPN]BF_4$[1], respectively, with KF (1.05 eq) in anhydrous MeOH.[3] The work-up was performed similar to the procedure for **1** described in the main text. Demethylation of Me_2CO_3 can be performed analogously to yield the methylcarbonates **2-PPN**, **2-PPNMe$_2$** and **2-TBA.**

Single crystals for XRD structure determination could be grown from a solution in acetonitrile and diethyl ether. **2-PPN** crystallizes in the monoclinic space group *P*21/*c* with eight ion pairs and four molecules of acetonitrile per unit cell (See crystallographic data chapter). Each anion is surrounded by four PPN cations or by PPN cation and one acetonitrile molecule, respectively. The H-bonds are reaching from 2.34 Å to 2.50 Å. Each oxygen atom of the methylcarbonate anions is bonded either to C-H acidic positions of the cation or of the solvent acetonitrile via H-bonds. Thereby each terminal oxygen atom acts as H-bond acceptor. There are no P···O interactions between methylcarbonate anion and cation. The distance C77-H77A···O1 of the interacting solvent acetonitrile is observed at 2.41 Å. CH-activation with methylcarbonate salts is commonly observed for imidazolium-cations.[4]

Single crystals for XRD structure determination could be grown from a solution in acetonitrile and diethyl ether. **2-PPNNMe$_2$** crystallizes in the triclinic space group $P\bar{1}$ with two ion pairs per unit cell (Figure 3). Each methylcarbonate anion is attached to four $PPNMe_2$ cations forming H-bonds to methyl group protons from 2.48 Å to 2.50 Å.

Despite our concerns with respect to a potentially limited hydrolytic stability of the methylcarbonate anion, we also successfully converted the most common organic fluoride salt as trihydrate TBA[F] · 3 H_2O into $TBA[OCO_2Me]$ (**2-TBA**) by this method. This implies that the methylcarbonate anion is not very sensitive – even at 140°C - towards minor amounts of H_2O in large excess of MeOH. However, the in situ generation of TBA[F] in methanol from $TBA[BF_4]$ by the described method works as well, if rigorous exclusion of any water potentially hydrogen bridge bonded to the methylcarbonate anion must be avoided. Water is stronger binding and more difficult to be fully removed than methanol.

*Synthesis of $PPNMe_2[OCO_2Me]$ (**2-PPNMe$_2$**)*

In a glass autoclave with 5mm thick glass and QVF high-pressure (25 bar) teflon valve $[(Me_2N)_3P{=}N{=}P(NMe_2)_3]F$ (**1-PPNMe$_2$**) (2.57 g, 0.007 mol, 1.00 eq.) was diluted with a mixture of Me_2CO_3 (4 mL, 0.048 mol, 6.80 eq.) and MeOH (1 mL). The reaction mixture was stirred for 3 days at 140 °C. A large amount of **2-PPNMe$_2$** was already crystalized in the autoclave and were filtered off. All volatiles were removed from filtrate in fine vacuum until a colorless residue is obtained. MeCN is added to this residue until a clear solution is obtained. To this solution diethyl ether is added slowly until the precipitation of product begins. The solution is stored at –30 °C for crystallization. The colorless needles

can be isolated by filtration, and the mother liquor can be collected for further crystallization steps. **2-PPNMe$_2$** is obtained in a yield of 2.18 g (0.005 mol, 75%). **^{1}H-NMR** (300.19 MHz, dmso-d$_6$): δ = 3.19 (s, 3H, [OCO$_2$C*H*$_3$]$^-$), 2.63-2.59 (m, 36H, N*Me*$_2$) ppm. **^{13}C-NMR** (75.48 MHz, dmso-d$_6$): δ = 36.2 (m, 36C, N*Me*$_2$), 50.8 (s, [OCO$_2$*C*H$_3$]$^-$) ppm. **Elemental analysis** found (calcd.) (%) for $C_{14}H_{39}N_7O_3P_2$ (415.5 g mol^{-1}): 40.5 (40.5), 9.4 (9.5).

*Synthesis of PPN[OCO$_2$Me] · 0.5 MeCN (**2-PPN · 0.5 MeCN**)*

The synthesis was performed analogously to the preparation of **2** using PPN[F] (9.36 g, 16.8 mmol, 1.0 eq.), Me_2CO_3 (20 mL, 0.24 mol, 14.3 eq.), and MeOH (5 mL) and stirring the reaction mixture for 5 days at 140°C. **2-PPN · 0.5 MeCN** is obtained with a yield of 7.19 g (11.3 mmol, 67%). **^{1}H-NMR** (300.13 MHz, dmso-d$_6$): δ = 7.71-7.51 (m, 30H, [N(P*Ph*$_3$)$_2$]$^+$), 3.15 (s, 3H, [OCO$_2$C*H*$_3$]$^-$), 2.07 (s, 1.5H, 0.5 x *H*$_3$CCN) ppm. **^{13}C-NMR** (75.48 MHz, dmso-d$_6$): δ = 155.4 (s, [O*C*O$_2$CH$_3$]$^-$), 133.6 (s*) & 131.9 (m*) & 129.5 (m*) & 126.8 (dd, $^1J_{CP}$ = 107.6 Hz, $^2J_{CN}$ = 2.5 Hz) (signals for the PPN$^+$ cation), 118.0 (s*, H$_3$C*C*N), 50.7 (s, [OCO$_2$*C*H$_3$]$^-$), 1.1 (s, H$_3$*C*CN) ppm. *The expected multiplet could not be resolved as the intensity of the corresponding signals is too low. **Elemental analysis** found (calcd.) (%) for $C_{39}H_{34.5}N_{1.5}O_3P_2$ (634.2 g mol^{-1}): C 73.3 (73.9), H 5.5 (5.5), N 3.6 (3.3).

*Synthesis of TBA[OCO$_2$Me] (**2-TBA**)*

The synthesis of **2-TBA** was performed analogously to the preparation of **2**, using TBAF · 3 H$_2$O (3.10 g, 9.83 mmol, 1.0 eq.), Me_2CO_3 (9 mL, 0.11 mol, 11.2 eq.), and MeOH (5 mL) and stirring the reaction mixture for 3 days at 140°C. **2-TBA** is obtained with a yield of 2.30 g (7.24 mmol, 74%). **^{1}H-NMR** (300.13 MHz, dmso-d$_6$): δ = 3.18 (t, $^3J_{HH}$ = 3.8 Hz, 8H*, [N(C*H*$_2$CH$_2$CH$_2$CH$_3$)$_4$]$^+$), 3.15 (s, 3H*, [OCO$_2$C*H*$_3$]$^-$), 1.57 (pent., $^3J_{HH}$ = 7.7 Hz, 8H [N(CH$_2$C*H*$_2$CH$_2$CH$_3$)$_4$]$^+$), 1.31 (sext., $^3J_{HH}$ = 7.5 Hz, 8H [N(CH$_2$CH$_2$C*H*$_2$CH$_3$)$_4$]$^+$), 0.93 (t, $^3J_{HH}$ = 7.4 Hz 12H) ppm. *As the signals for the methylcarbonate anion and the *N*-attached methylene-groups coincide, only the sum of the integrals of these signals is accessible that equals 11. **^{13}C-NMR** (75.48 MHz, dmso-d$_6$): δ = 155.4 (s, [O*C*O$_2$CH$_3$]$^-$), 57.5 (t, $^1J_{CN}$ = 3.2 Hz, [N(*C*H$_2$CH$_2$CH$_2$CH$_3$)$_4$]$^+$), 50.7 (s, [OCO$_2$*C*H$_3$]$^-$), 23.0 (s, [N(CH$_2$*C*H$_2$CH$_2$CH$_3$)$_4$]$^+$), 19.2 (s, [N(CH$_2$CH$_2$*C*H$_2$CH$_3$)$_4$]$^+$), 13.4 (s, [N(CH$_2$CH$_2$CH$_2$*C*H$_3$)$_4$]$^+$) ppm. **Elemental analysis** found (calcd.) (%) for $C_{18}H_{39}NO_3$ (317.51 g mol^{-1}): C 68.2 (68.1), H 12.3 (12.4), N 4.6 (4.4). This method implies that the methylcarbonate anion is not sensitive towards minor amounts of H_2O. However, the *in situ* generation of TBA[F] in methanol from TBA[BF$_4$] by the described method works as well.

2. NMR-Spectra

*Ph_4PF (**1**)*

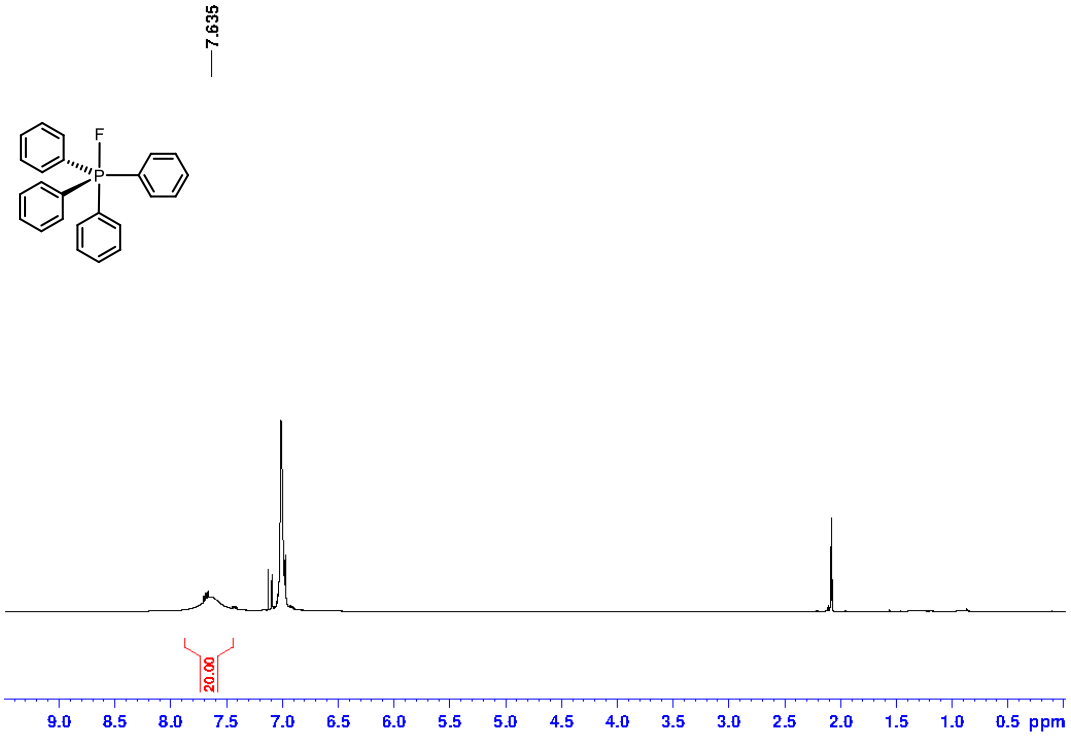

Figure S1. ^{1}H-NMR spectrum (300.1 MHz, toluene-d_8) of PPh_4F (**1**).

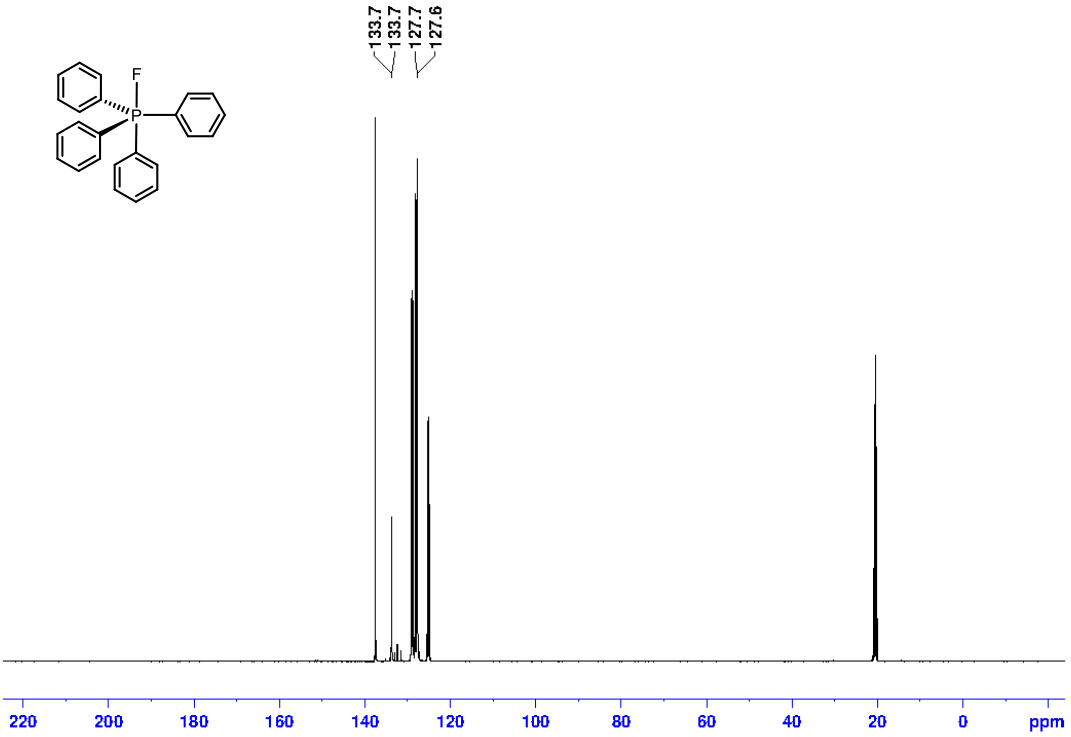

Figure S2. ^{13}C-NMR spectrum (75.5 MHz, toluene-d_8) of PPh_4F (**1**).

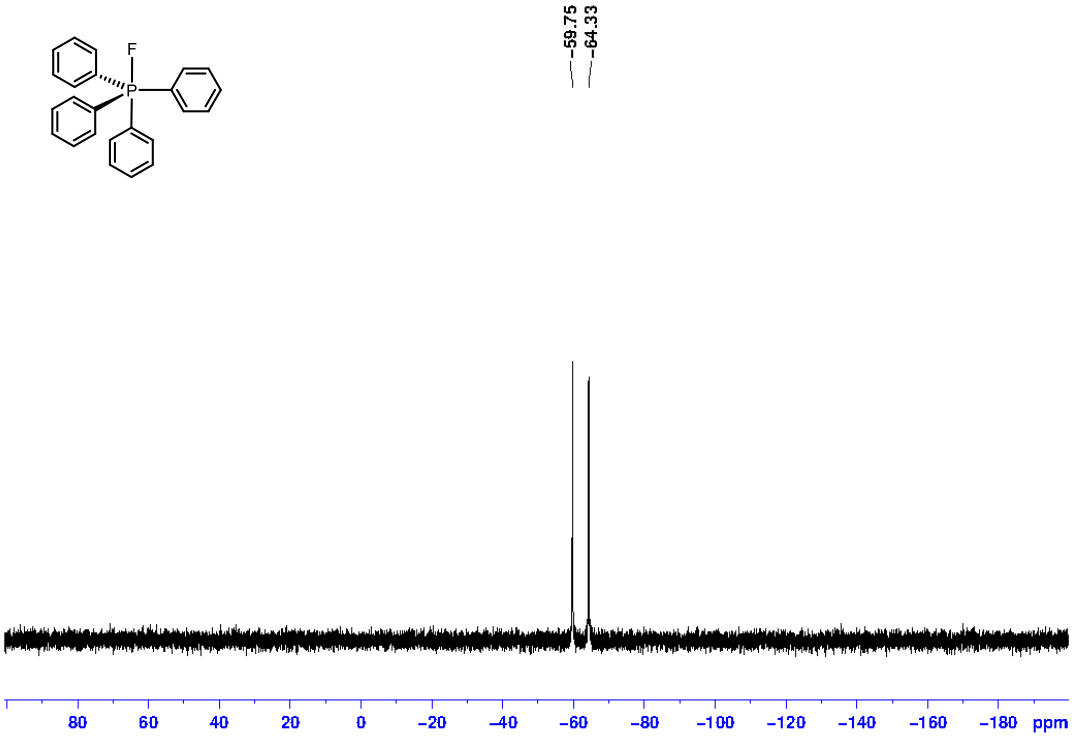

Figure S3. ^{31}P-NMR spectrum (122.5 MHz, toluene-d_8) of PPh_4F (**1**).

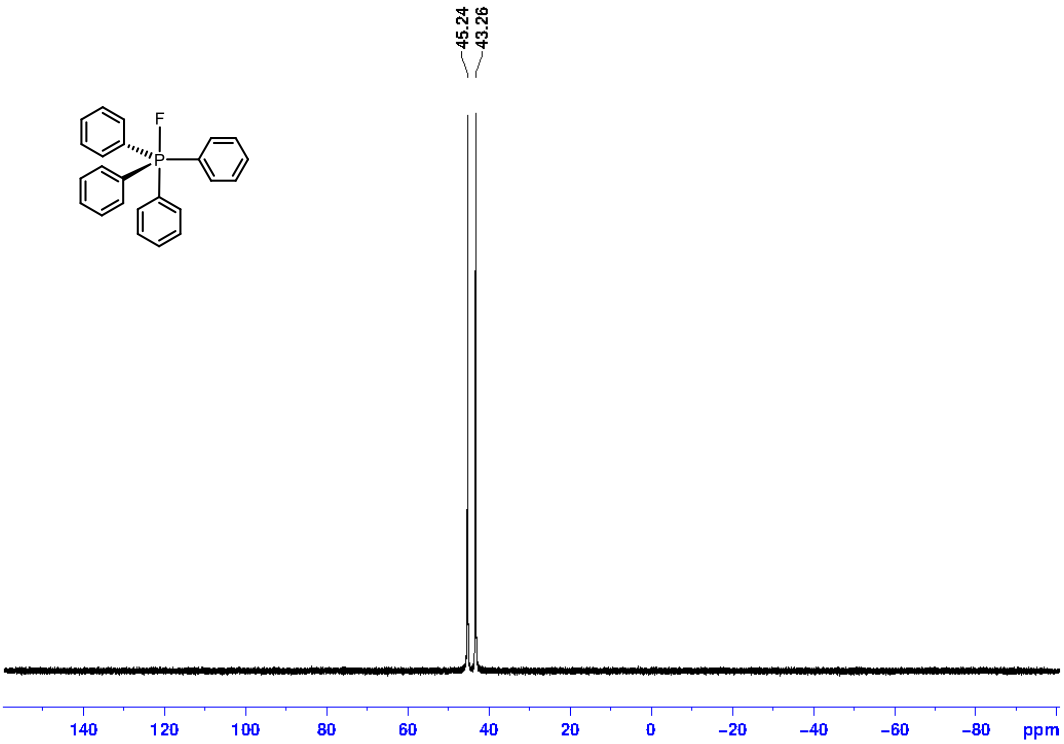

Figure S4. ^{19}F-NMR spectrum (282.5 MHz, toluene-d_8) of PPh_4F (**1**).

*$Ph_4P[OCO_2Me]$ (**2**)*

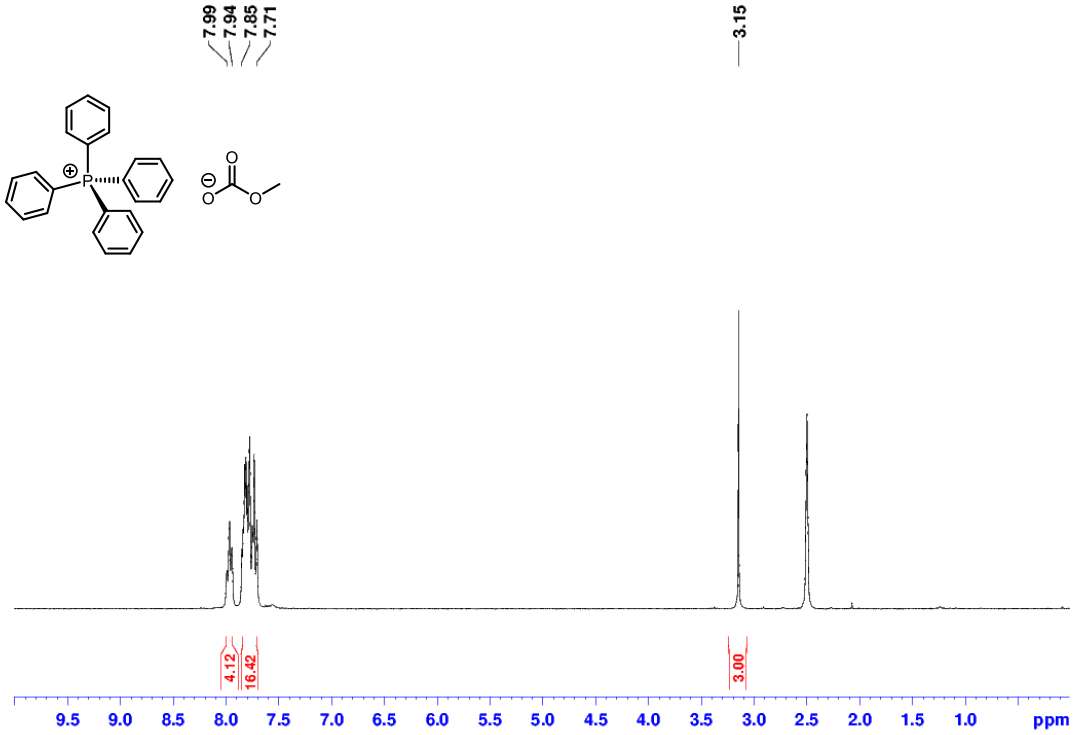

Figure S5. ^{1}H-NMR spectrum (300.1 MHz, dmso-d_6) of $PPh_4[OCO_2Me]$ (**2**).

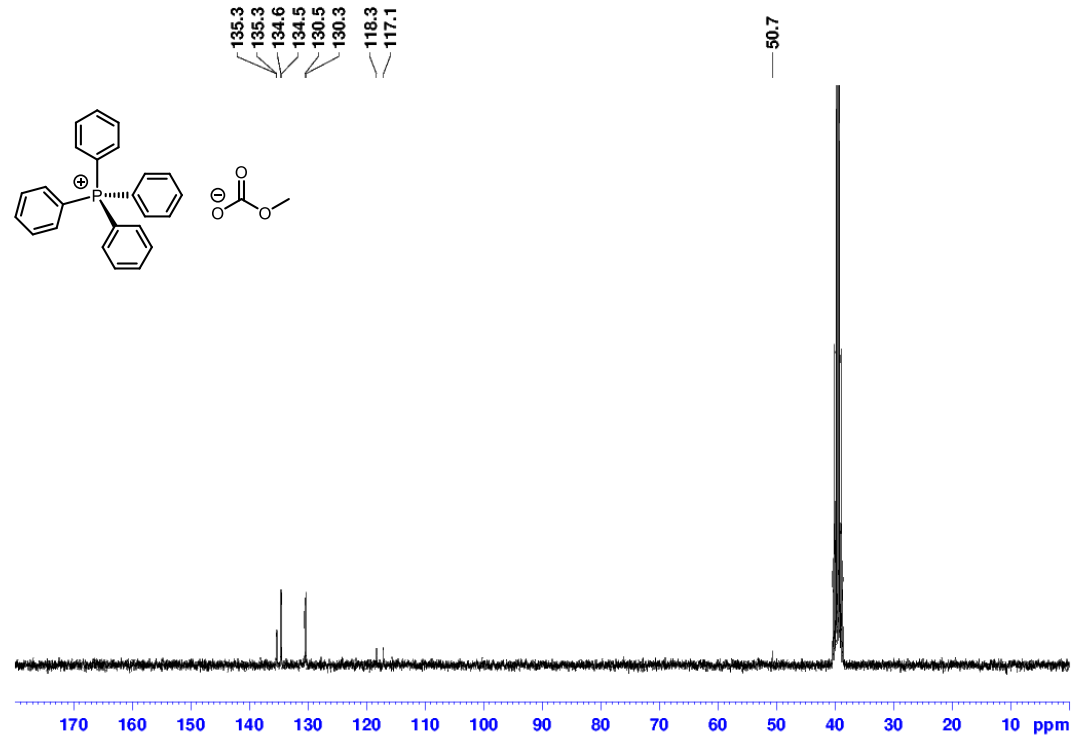

Figure S6. ^{13}C-NMR spectrum (75.5 MHz, dmso-d_6) of $PPh_4[OCO_2Me]$ (**2**).

*PPN[OCO_2Me] · 0.5 MeCN (**2-PPN**)*

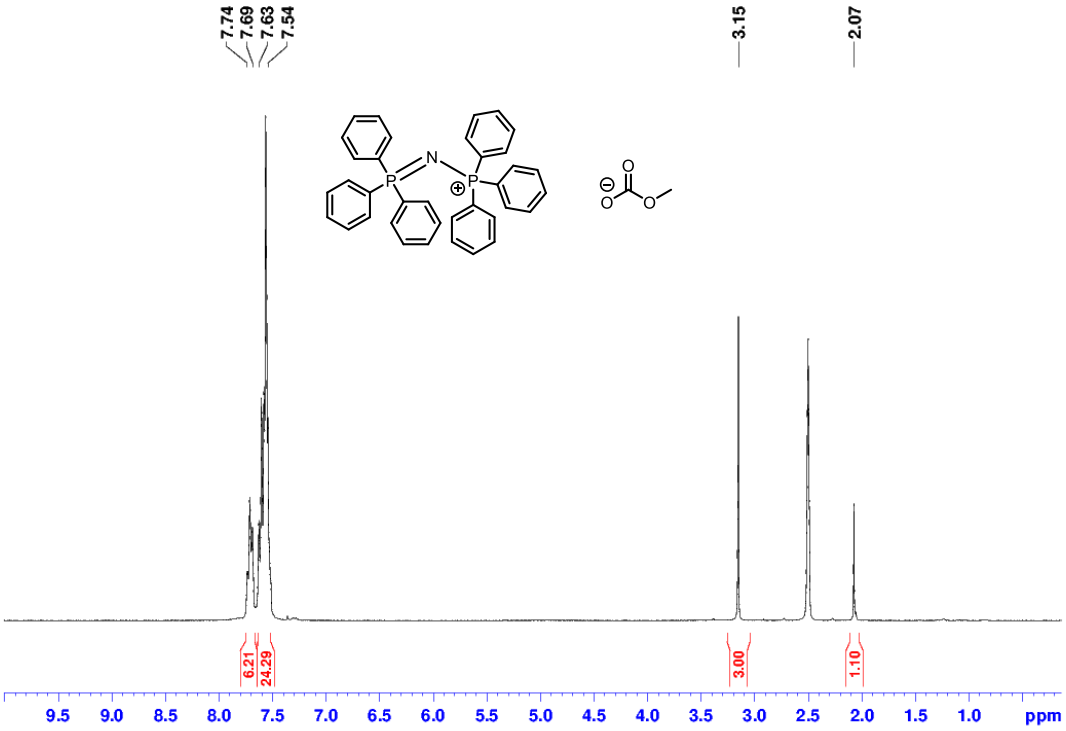

Figure S7. ^{1}H-NMR spectrum (300.1 MHz, dmso-d_6) of PPN[OCO_2Me] (**2-PPN**).

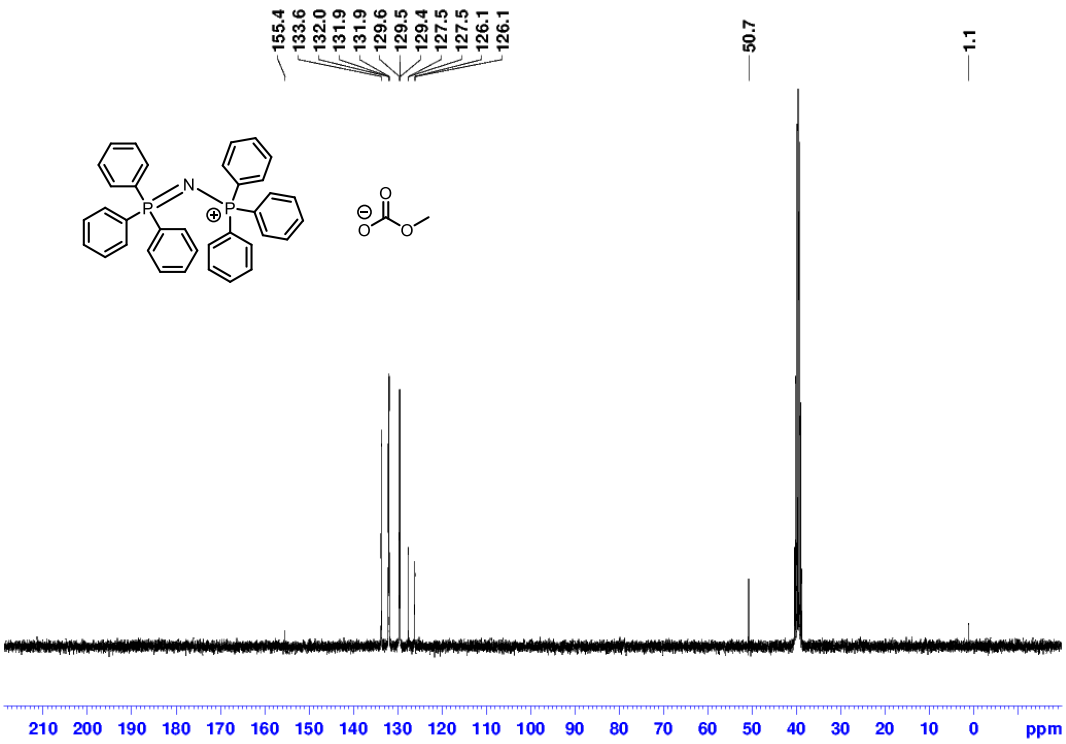

Figure S8. ^{13}C-NMR spectrum (75.5 MHz, dmso-d_6) of PPN[OCO_2Me] (**2-PPN**).

PPNMe$_2$[OCO$_2$Me] ***(2-PPNMe$_2$)***

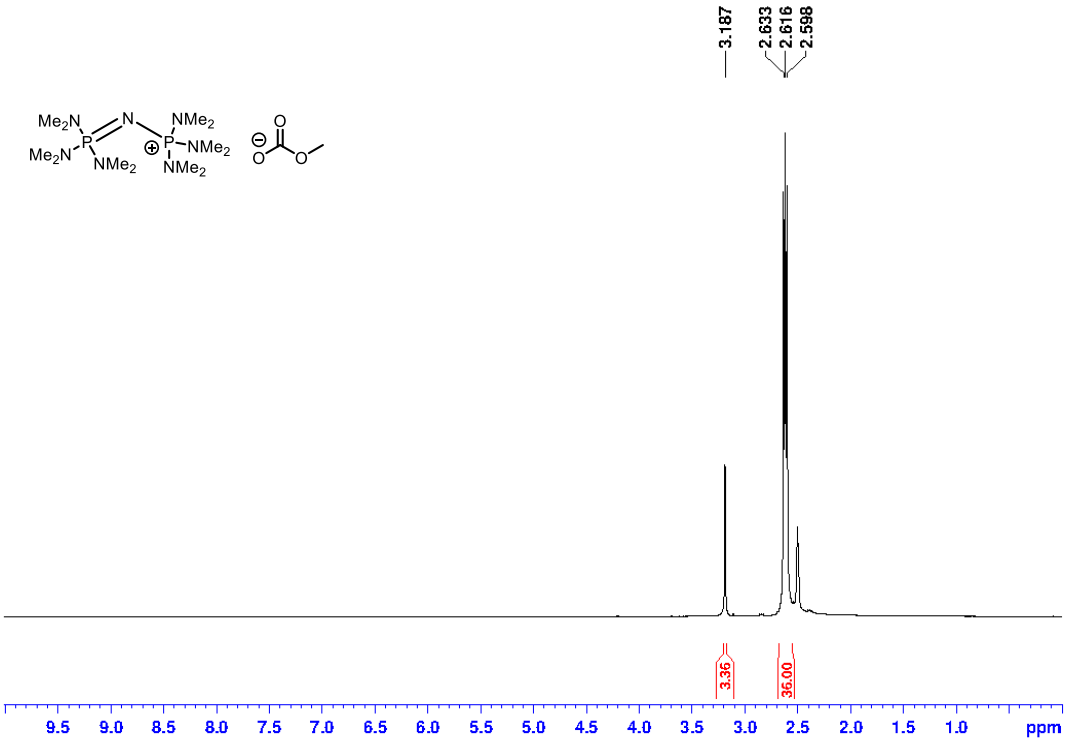

Figure S9. ^{1}H-NMR spectrum (300.1 MHz, dmso-d$_6$) of PPNMe$_2$[OCO$_2$Me] (**2-PPNNMe$_2$**).

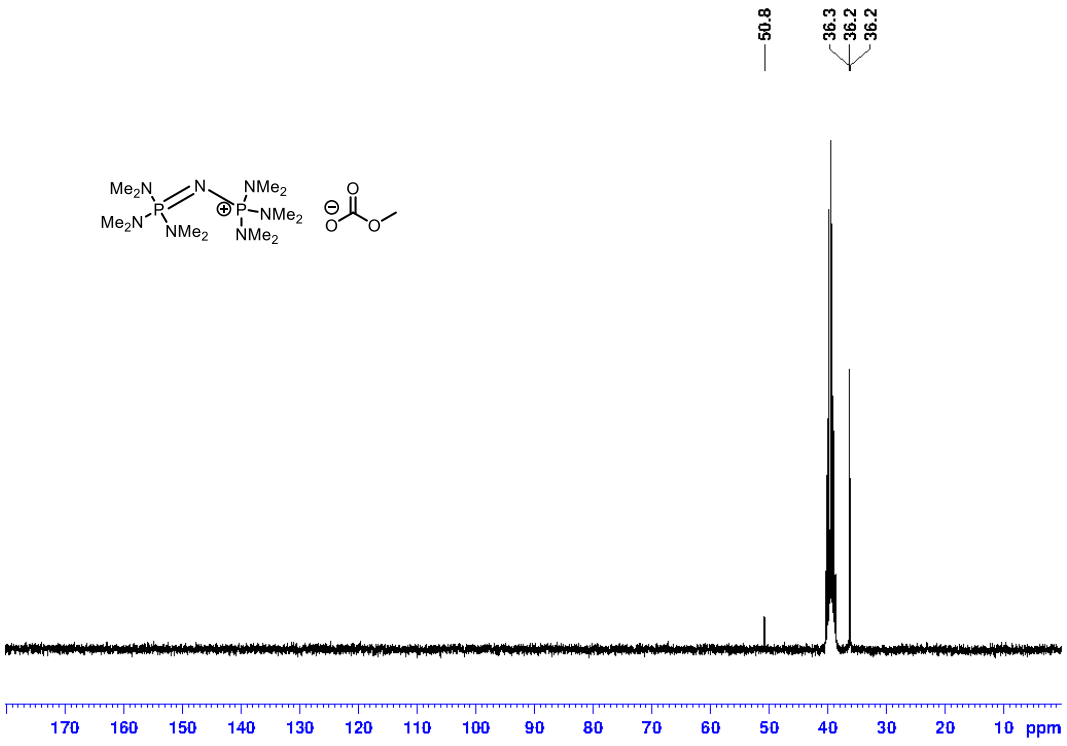

Figure S10. ^{13}C-NMR spectrum (75.5 MHz, dmso-d$_6$) of PPNMe$_2$[OCO$_2$Me] (**2-PPNNMe$_2$**).

*TBA[OCO$_2$Me] (**2-TBA**)*

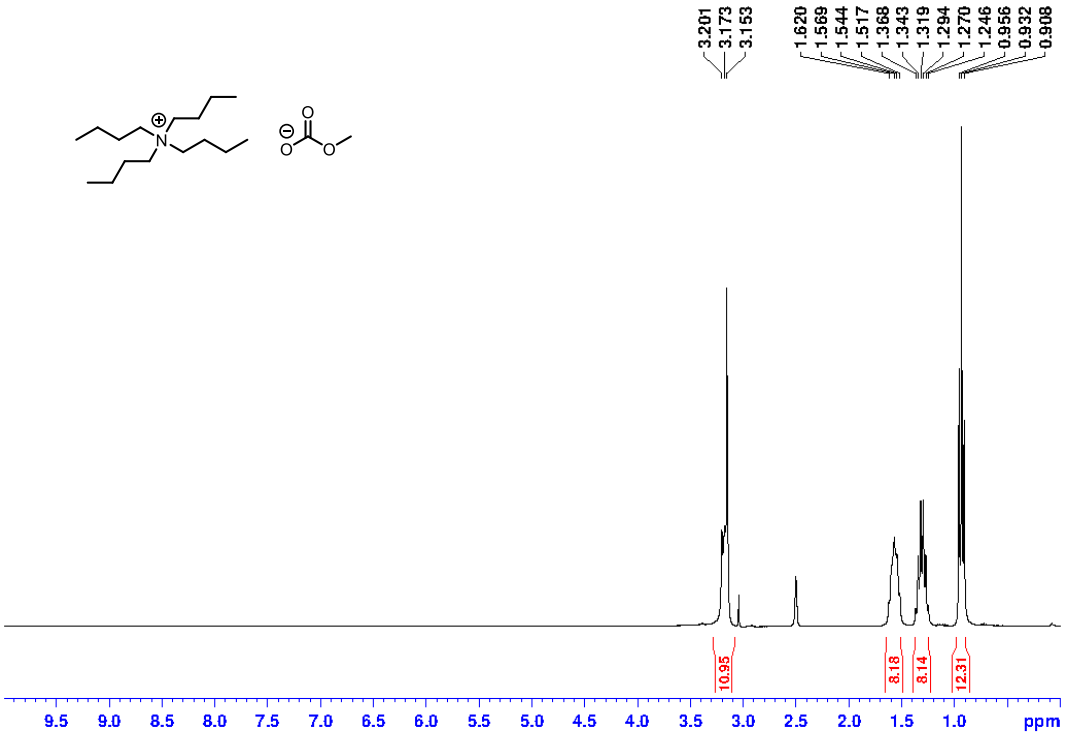

Figure S11. ^{1}H-NMR spectrum (300.1 MHz, dmso-d$_6$) of NBu$_4$[OCO$_2$Me] (**2-TBA**). Signals for the methylcarbonate anion and the N-attached methylene-groups coincide. The sum of the integrals of these signals equals the expected amount of 11.

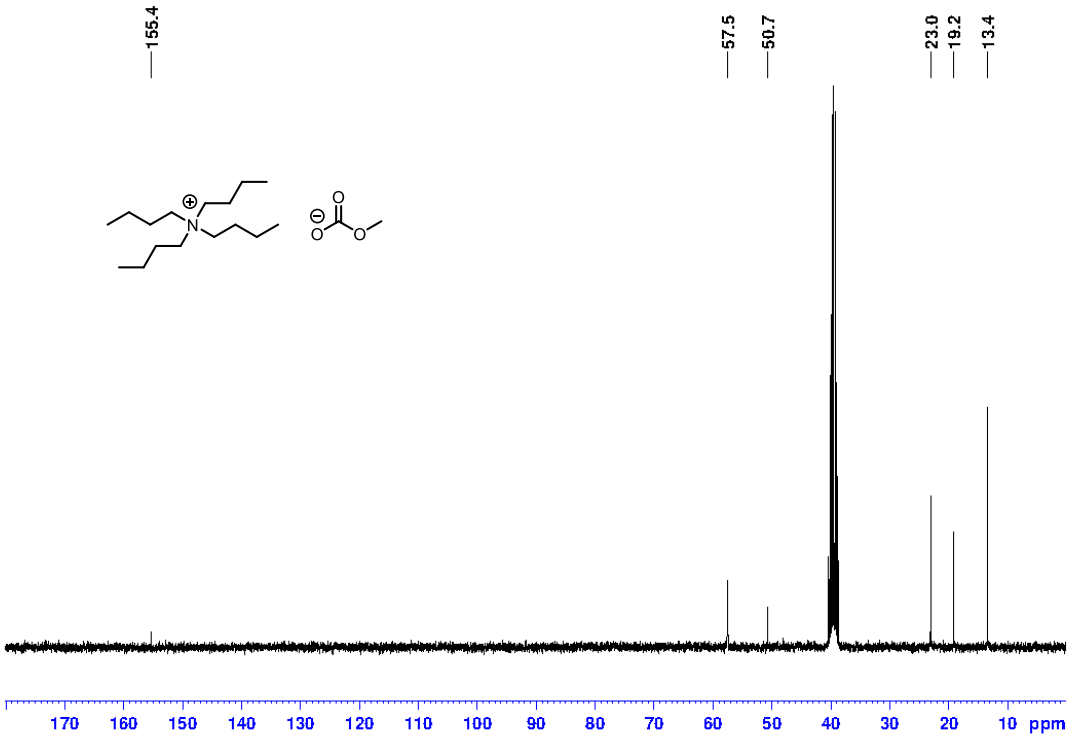

Figure S12. ^{13}C-NMR spectrum (75.5 MHz, dmso-d$_6$) of NBu$_4$[OCO$_2$Me] (**2-TBA**).

*$Ph_4P[SSiMe_3]$ (**3-S**)*

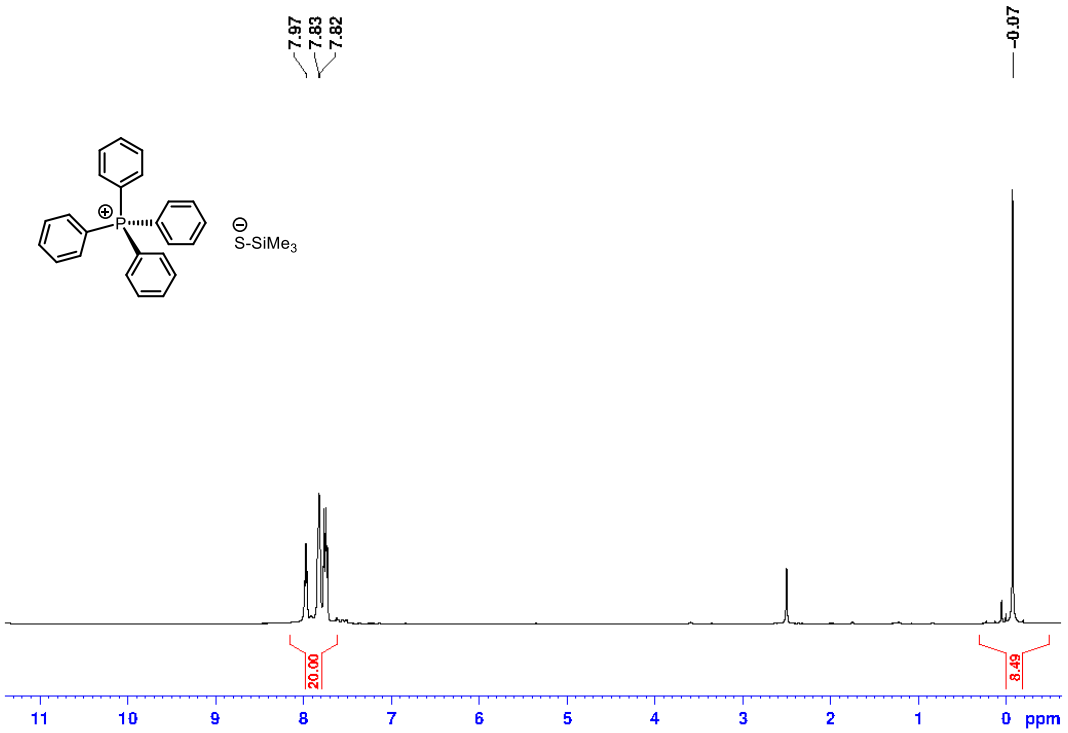

Figure S13. ^{1}H-NMR spectrum (300.1 MHz, dmso-d_6) of $PPh_4[SSiMe_3]$ (**3-S**).

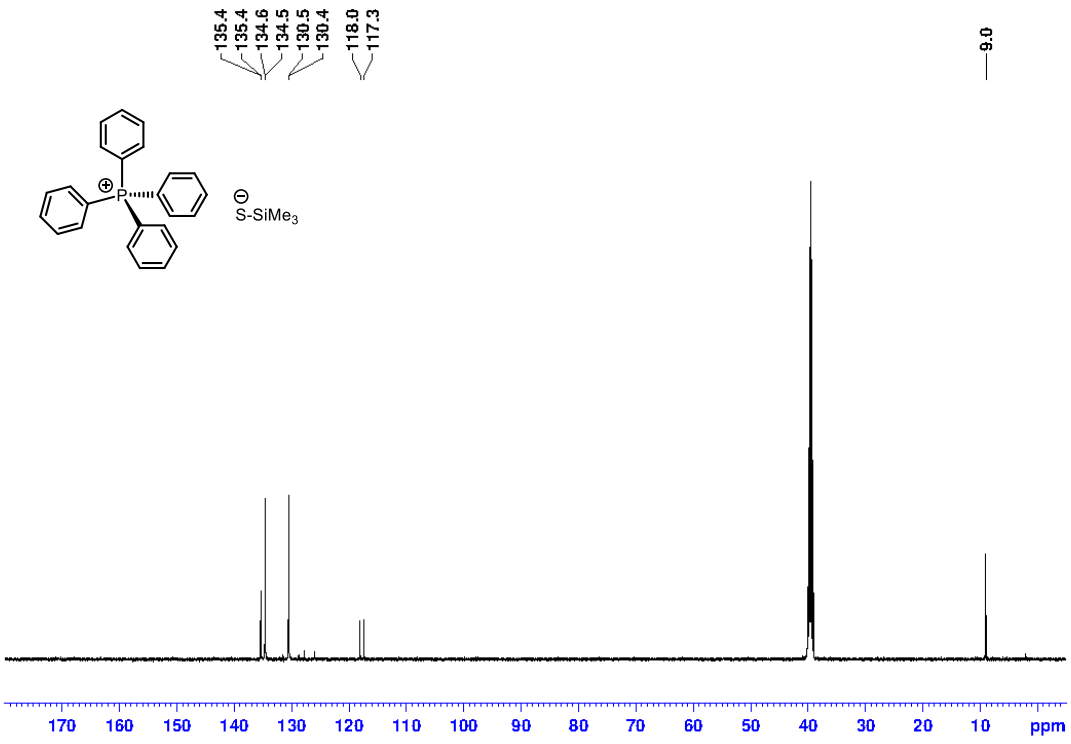

Figure S14. ^{13}C-NMR spectrum (75.5 MHz, dmso-d_6) of $PPh_4[SSiMe_3]$ (**3-S**).

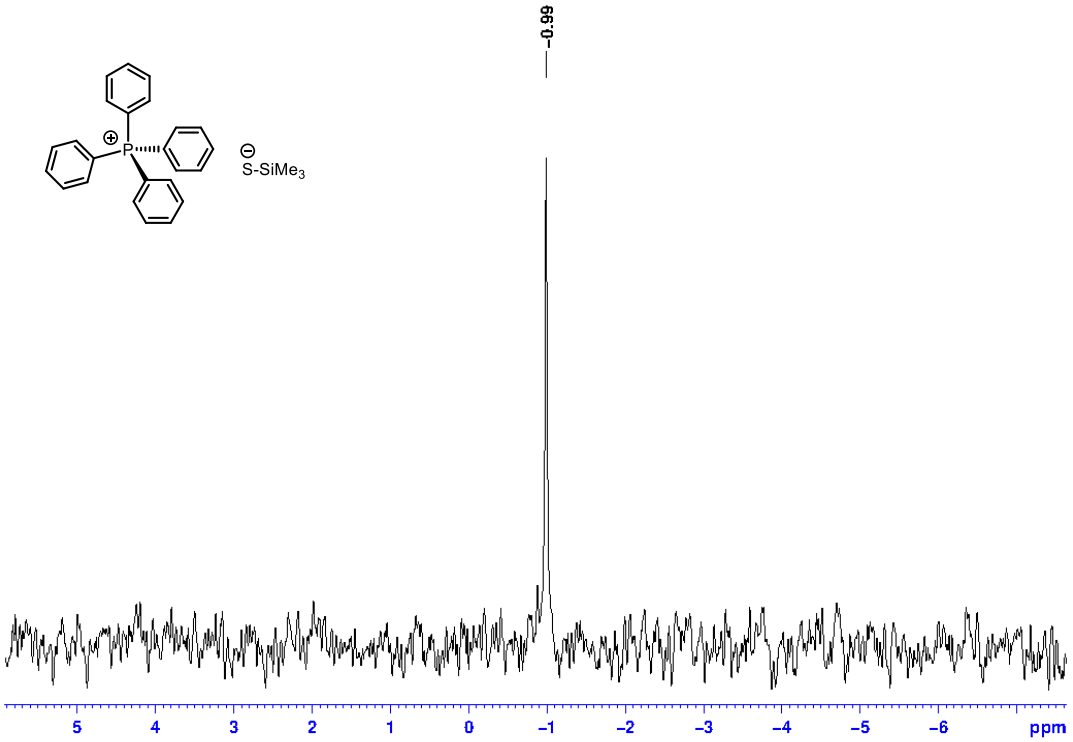

Figure 15. ^{29}Si-NMR spectrum (59.65 MHz, dmso-d_6) of $PPh_4[SSiMe_3]$ (**3-S**).

*$Ph_4P[SeSiMe_3]$ (**3-Se**)*

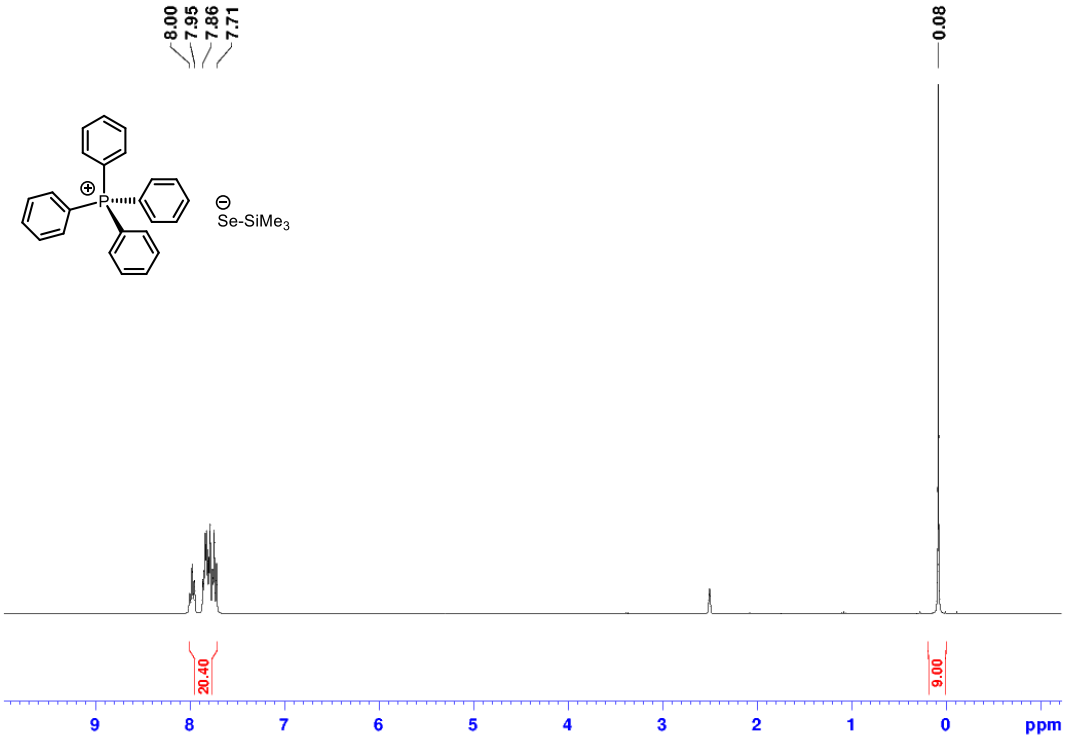

Figure S16. ^{1}H-NMR spectrum (300.1 MHz, dmso-d_6) of $PPh_4[SeSiMe_3]$ (**3-Se**).

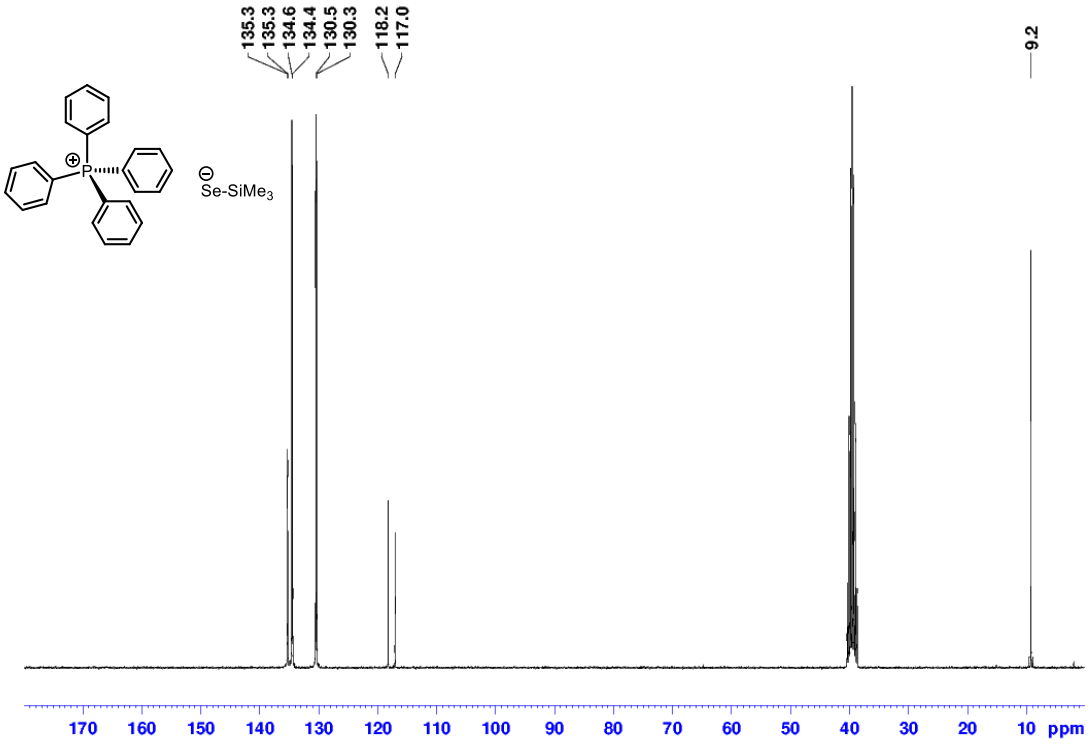

Figure S17. ^{13}C-NMR spectrum (75.5 MHz, dmso-d_6) of $PPh_4[SeSiMe_3]$ (**3-Se**).

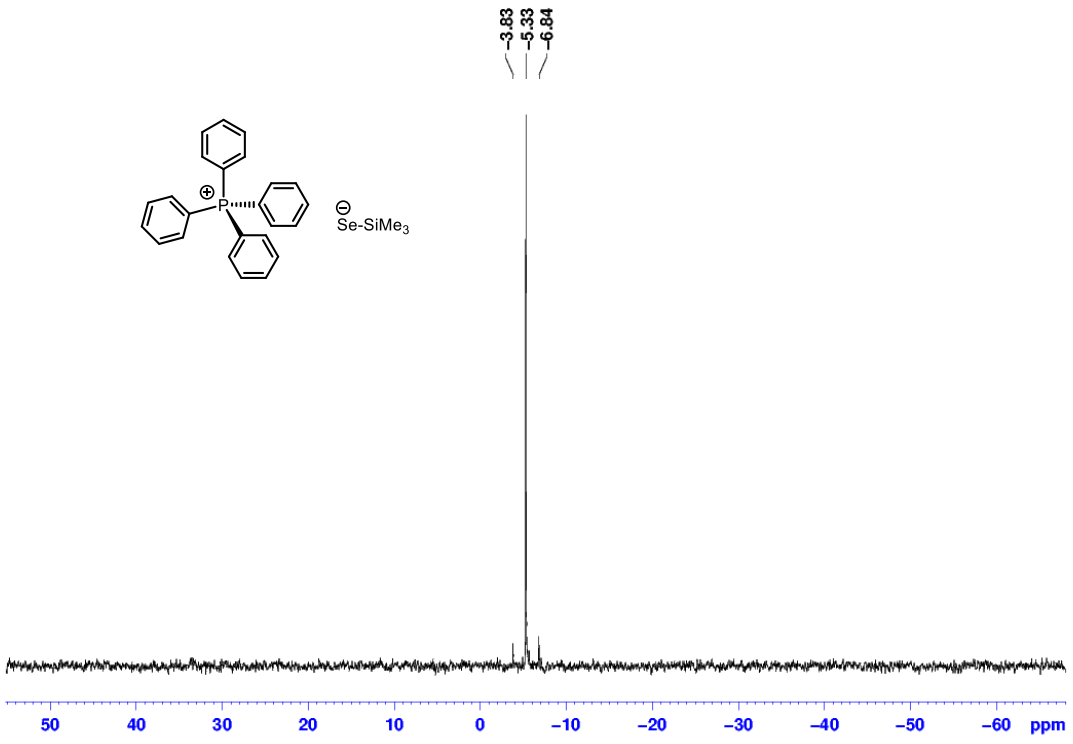

Figure S18. ^{29}Si-NMR spectrum (59.65 MHz, dmso-d_6) of $PPh_4[SeSiMe_3]$ (**3-Se**).

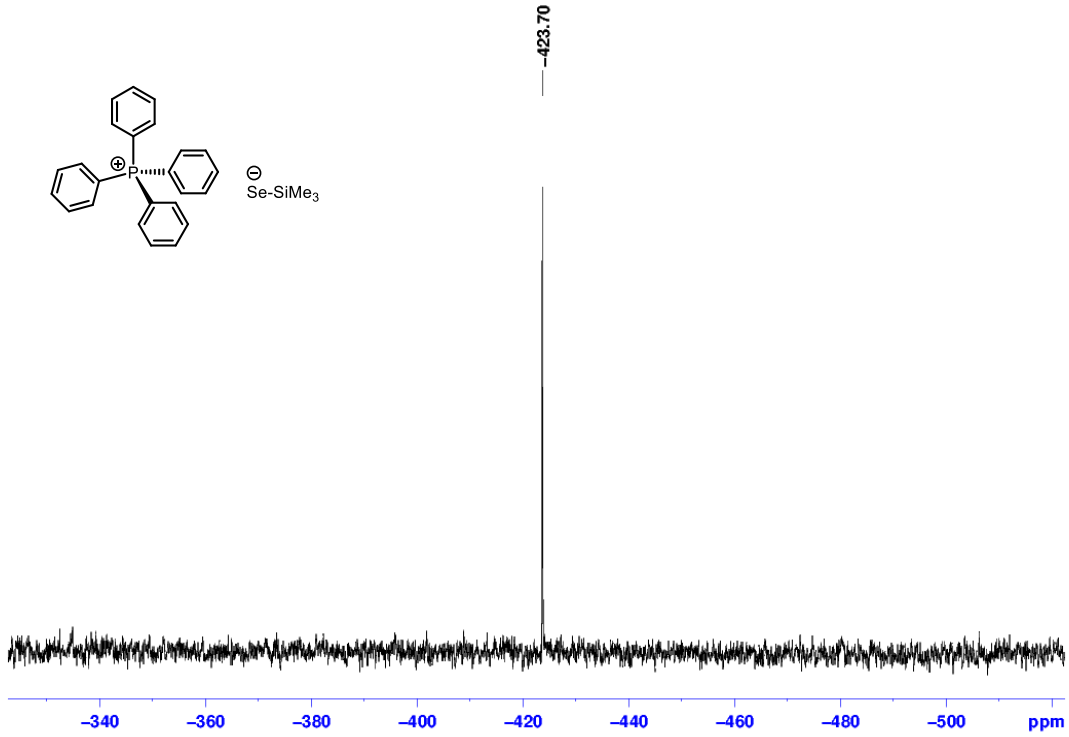

Figure S19. ^{77}Se-NMR spectrum (57.26 MHz, dmso-d_6).of $PPh_4[SeSiMe_3]$ (**3-Se**).

*$Ph_4P[TeSiMe_3]$ (**3-Te**)*

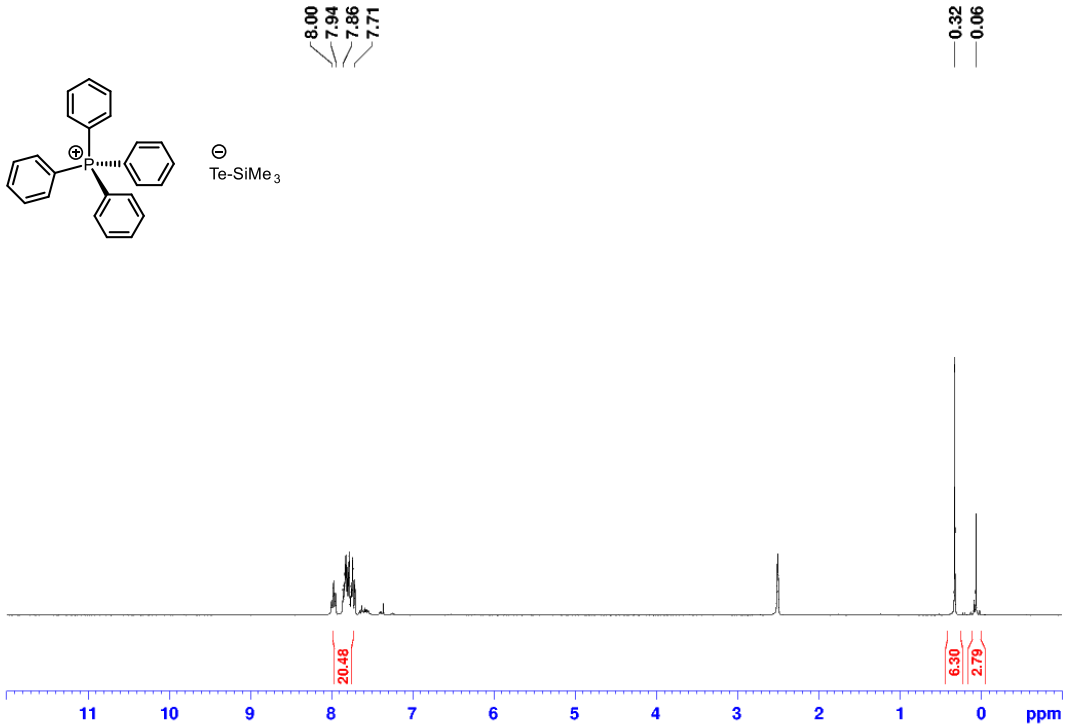

Figure S20. ^{1}H-NMR spectrum (300.1 MHz, dmso-d_6) of $PPh_4[TeSiMe_3]$ (**3-Te**). The signal at 0.06 ppm can be assigned to $O(SiMe_3)_2$ which arises due to diffusion of H_2O into the NMR-sample.

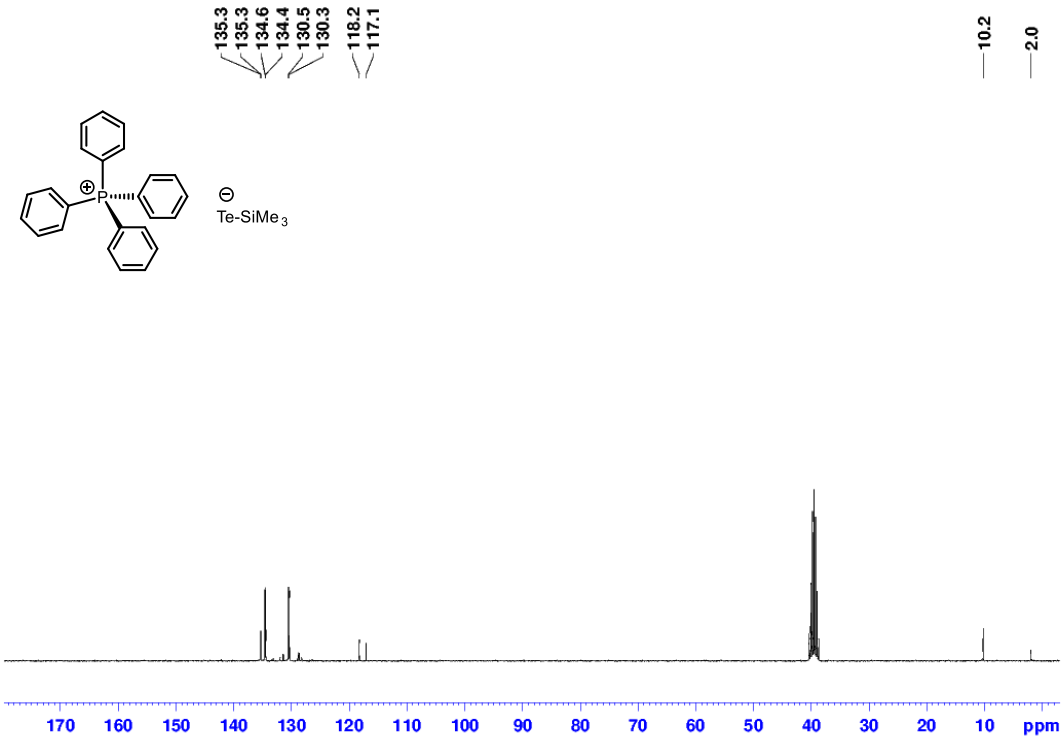

Figure S21. ^{13}C-NMR spectrum (75.5 MHz, dmso-d_6) of $PPh_4[TeSiMe_3]$ (**3-Te**).The signal at 2.0 ppm can be assigned to $O(SiMe_3)_2$ which arises due to diffusion of H_2O into the NMR-sample.

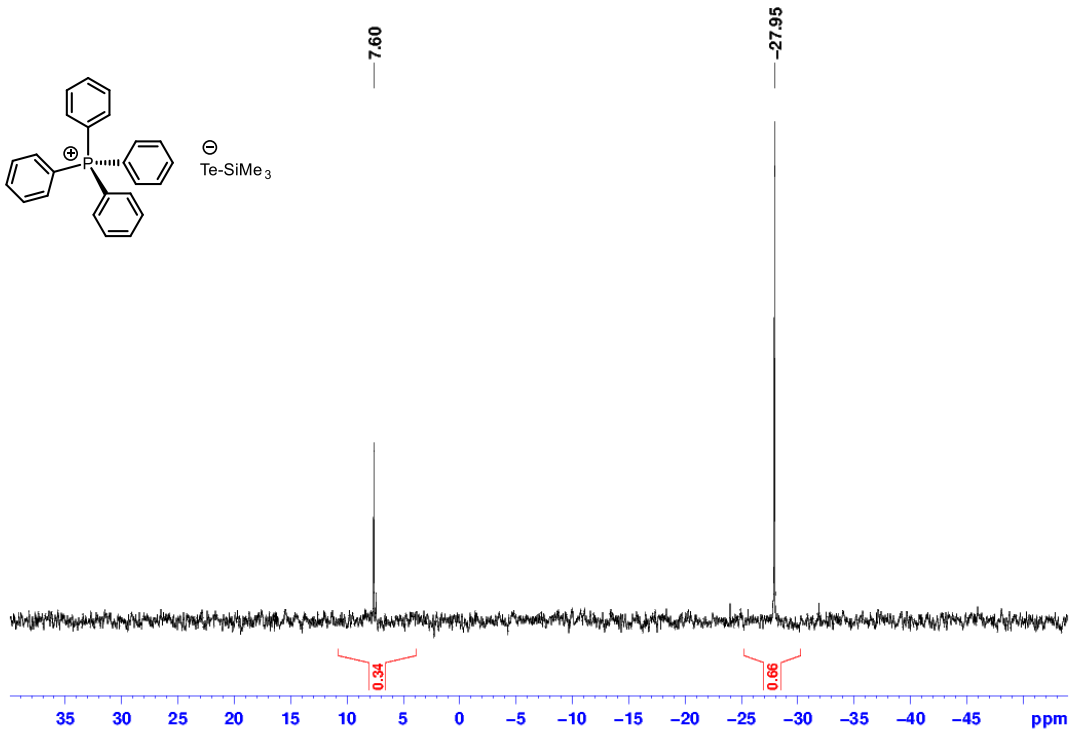

Figure S22. ^{29}Si-NMR spectrum (59.65 MHz, dmso-d_6) of $PPh_4[TeSiMe_3]$ (**3-Te**). The signal at 7.6 ppm can be assigned to $O(SiMe_3)_2$ which arises due to diffusion of H_2O into the NMR-sample.

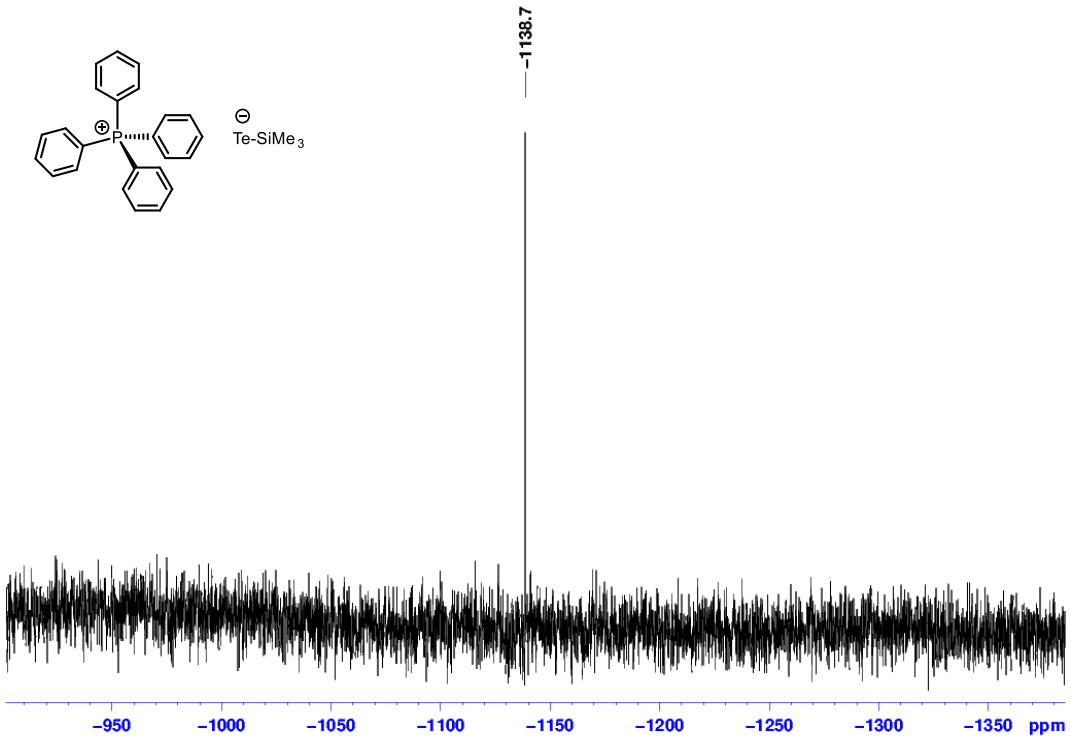

Figure S23. ^{125}Te-NMR spectrum (94.73 MHz, dmso-d_6) of $PPh_4[TeSiMe_3]$ (**3-Te**).

*$Ph_4P[Cp_3LaSSiMe_3]$ (**4-S**)*

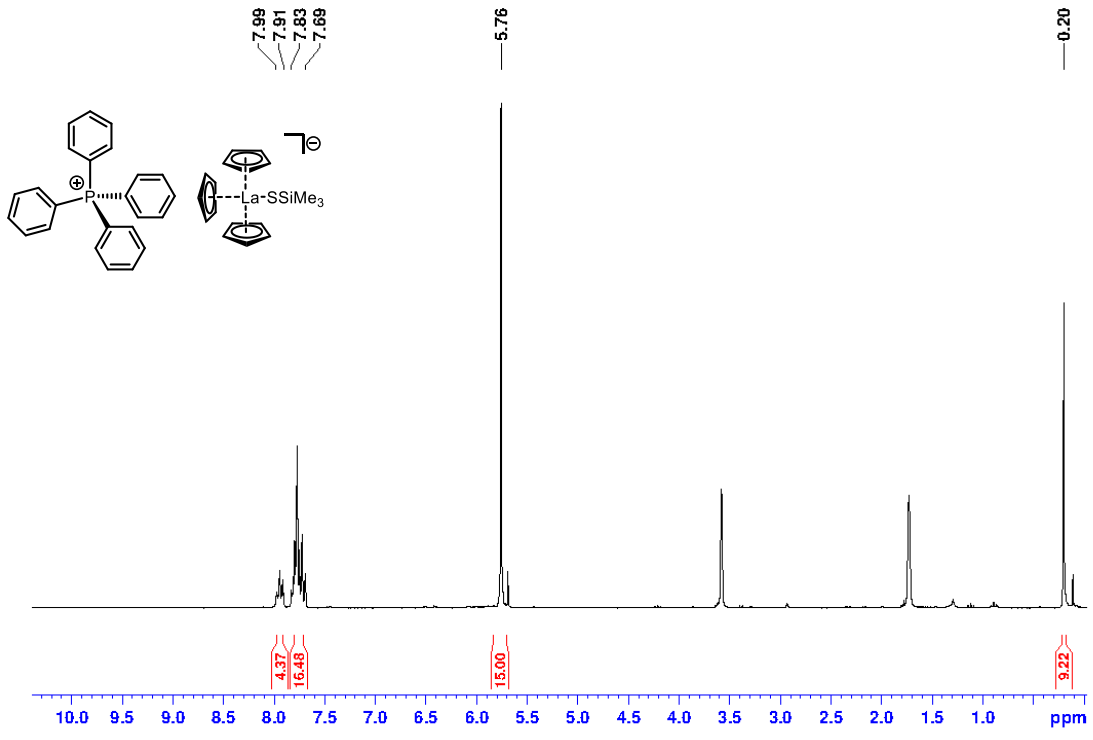

Figure S24. ^{1}H-NMR spectrum (300.25 MHz, thf-d_8) of $PPh_4[Cp_3LaSSiMe_3]$ (**4-S**).

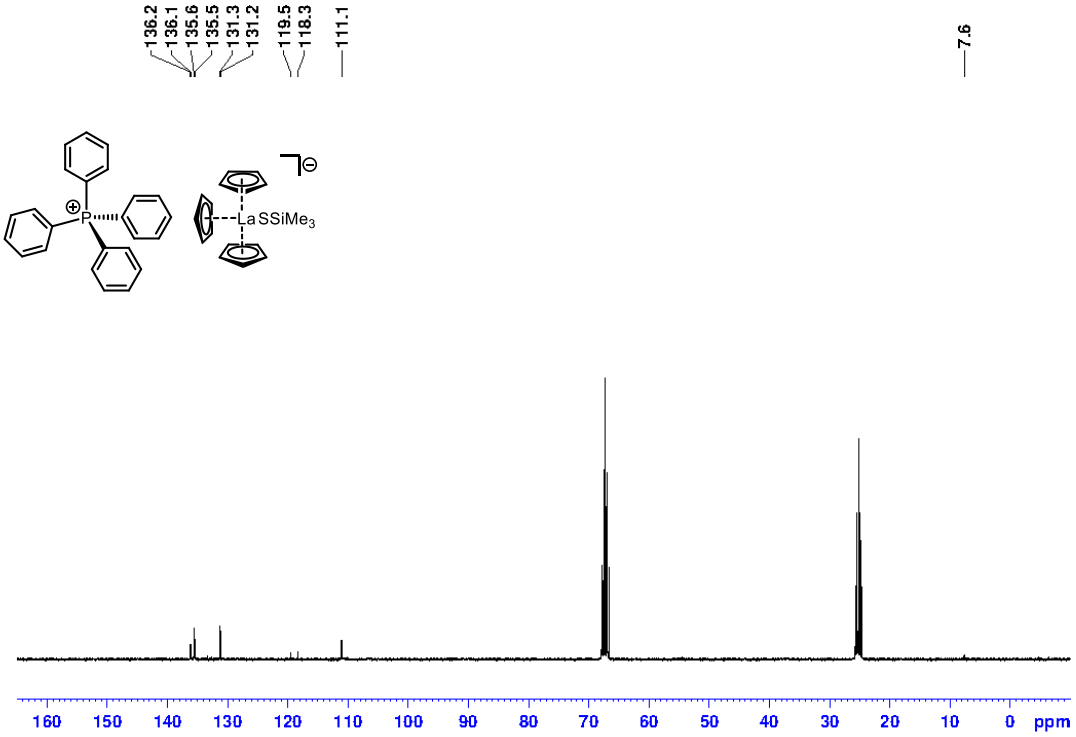

Figure S25. ^{13}C-NMR spectrum (75.5 MHz, thf-d_8) of $PPh_4[Cp_3LaSSiMe_3]$ (**4-S**).

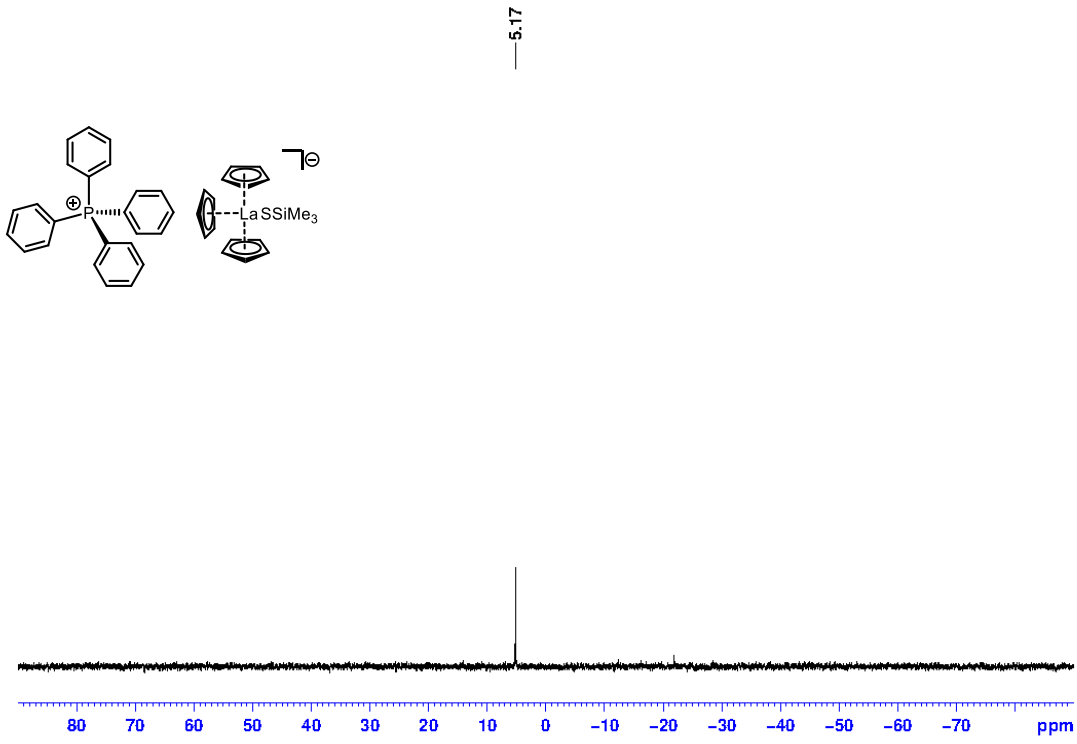

Figure S26. ^{29}Si-NMR spectrum (59.65 MHz, thf-d_8) $PPh_4[Cp_3LaSSiMe_3]$ (**4-S**).

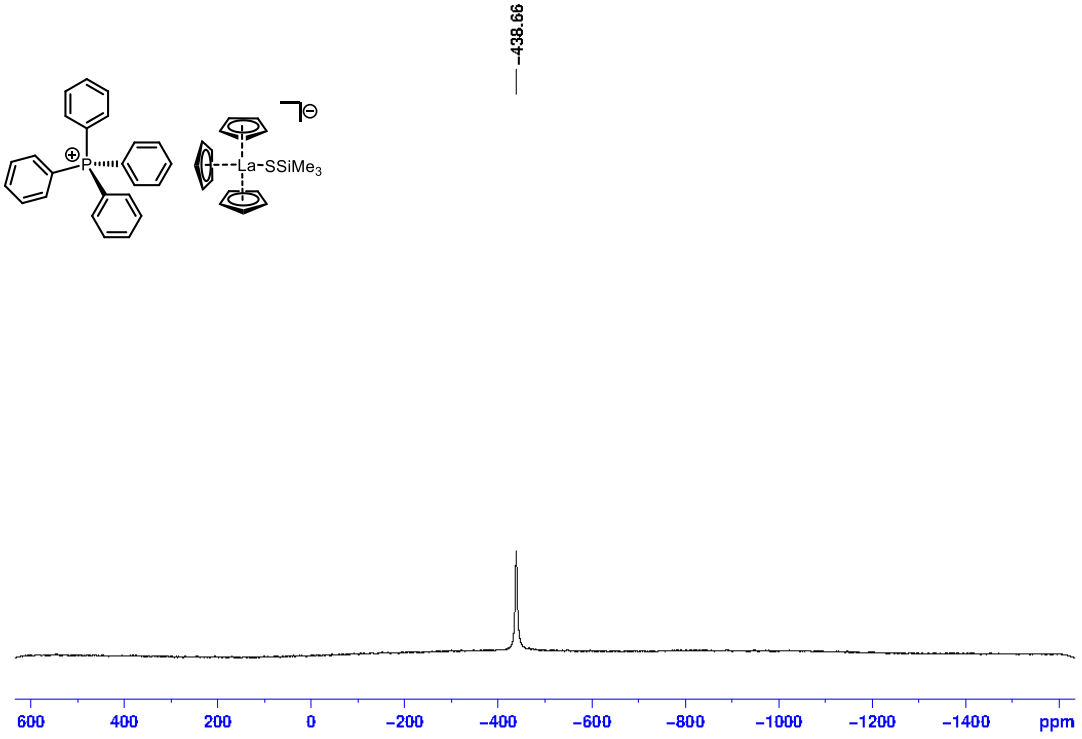

Figure S27. ^{139}La-NMR spectrum (42.41MHz, thf-d_8) $PPh_4[Cp_3LaSSiMe_3]$ (**4-S**).

*$Ph_4P[Cp_3LaSeSiMe_3]$ (**4-Se**)*

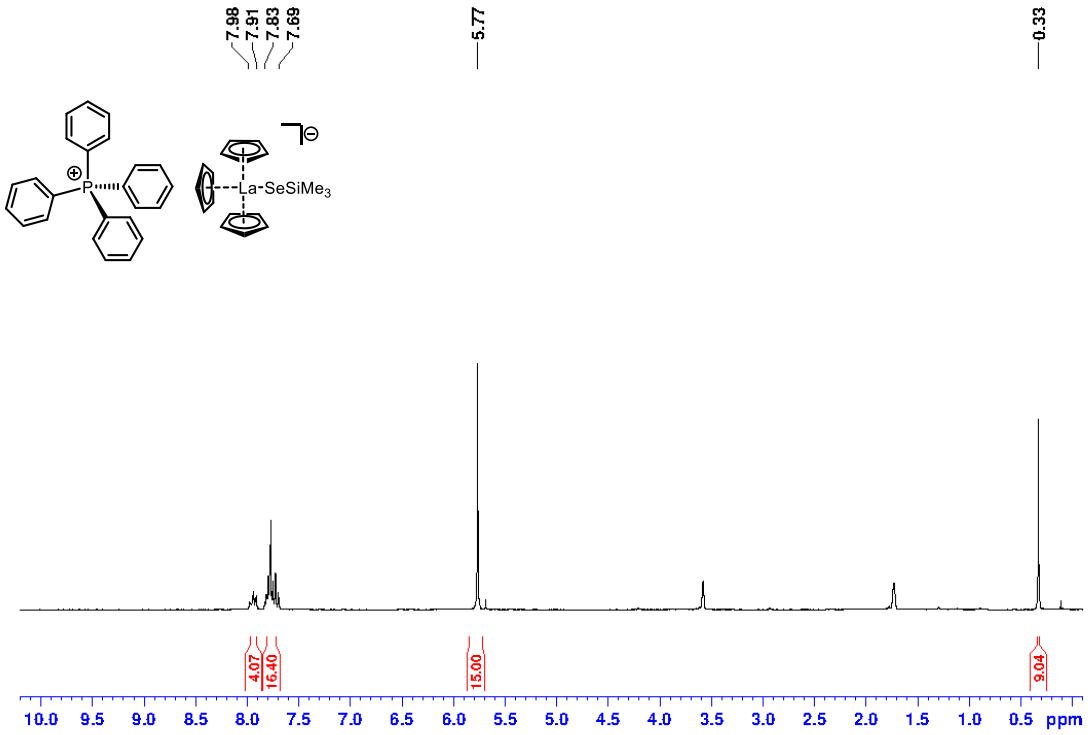

Figure S28. ^{1}H-NMR spectrum (300.25 MHz, thf-d_8) of $PPh_4[Cp_3LaSeSiMe_3]$ (**4-Se**).

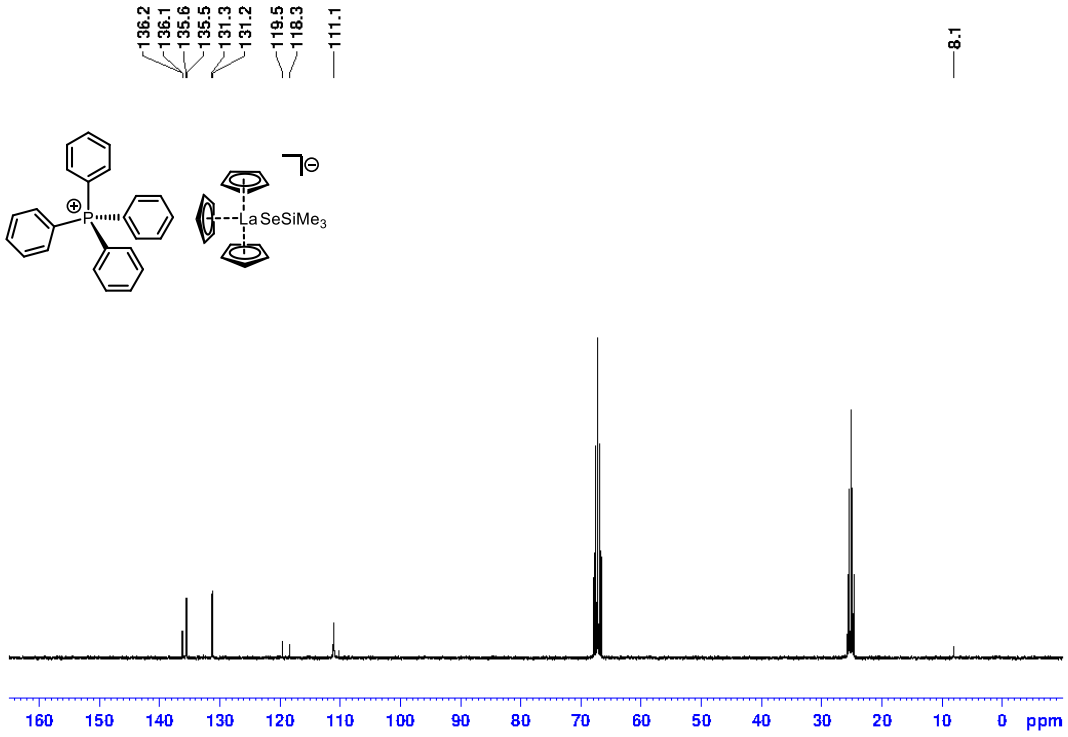

Figure S29. ^{13}C-NMR spectrum (75.5 MHz, thf-d_8) of $PPh_4[Cp_3LaSeSiMe_3]$ (**4-Se**).

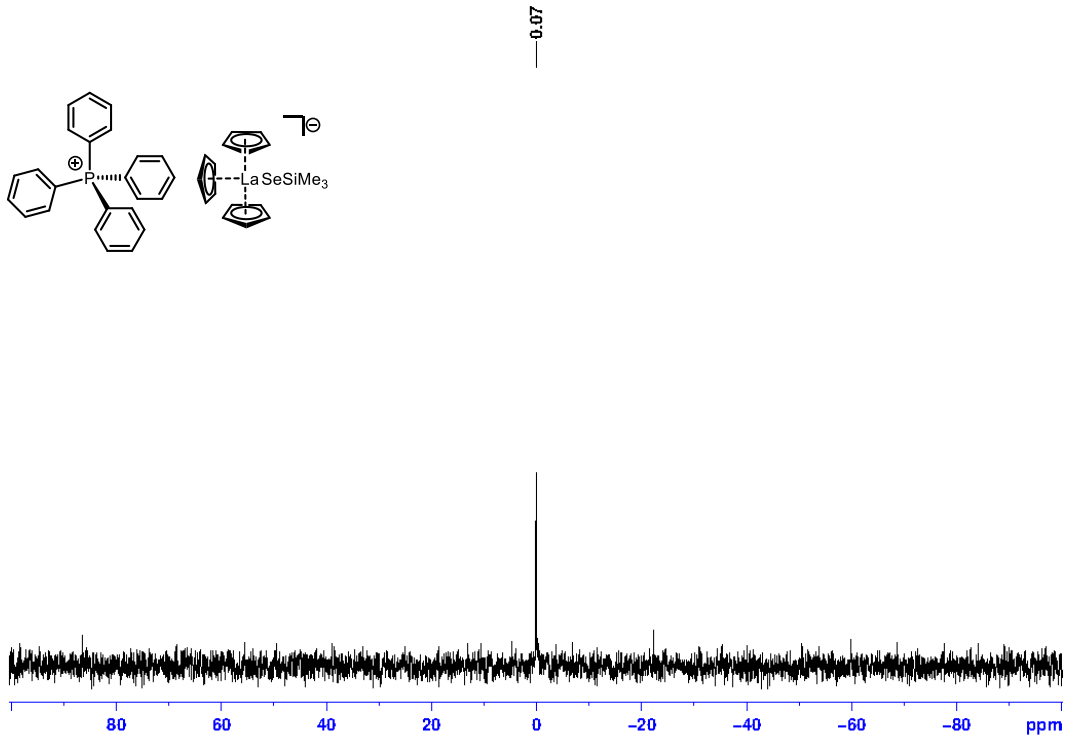

Figure S30. ^{29}Si-NMR spectrum (59.65 MHz, thf-d_8) $PPh_4[Cp_3LaSeSiMe_3]$ (**4-Se**).

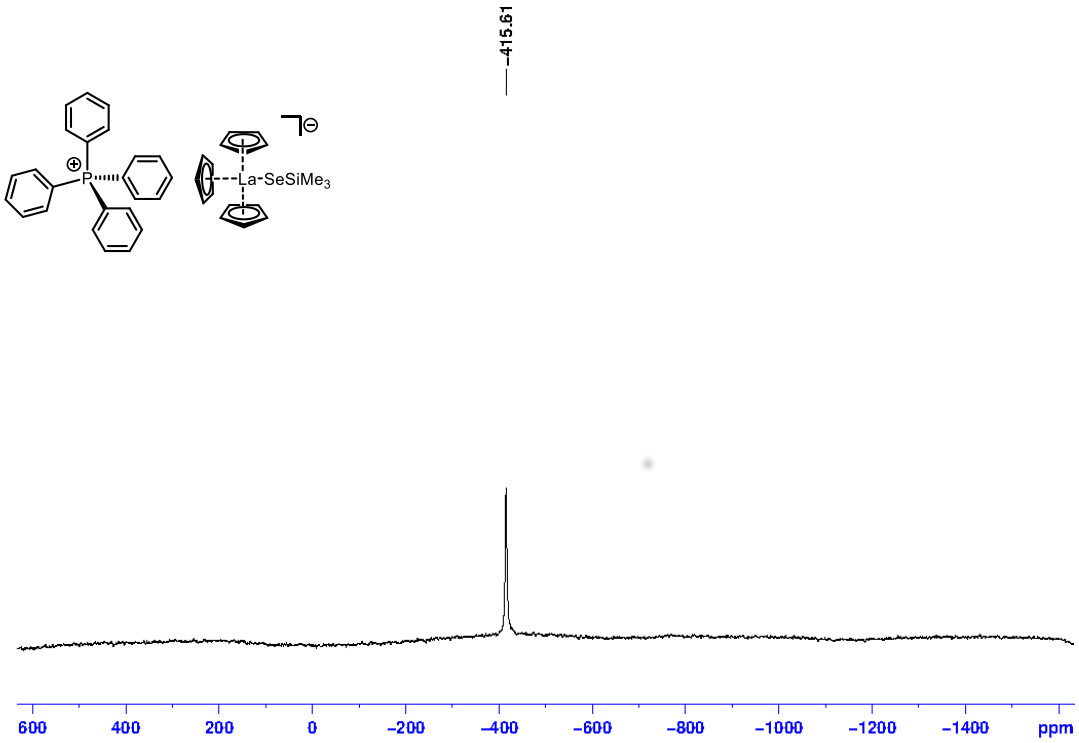

Figure S31. ^{139}La-NMR spectrum (42.41MHz, thf-d_8) $PPh_4[Cp_3LaSeSiMe_3]$ (**4-Se**).

*$Ph_4P[Cp_3LaTeSiMe_3]$(**4-Te**)*

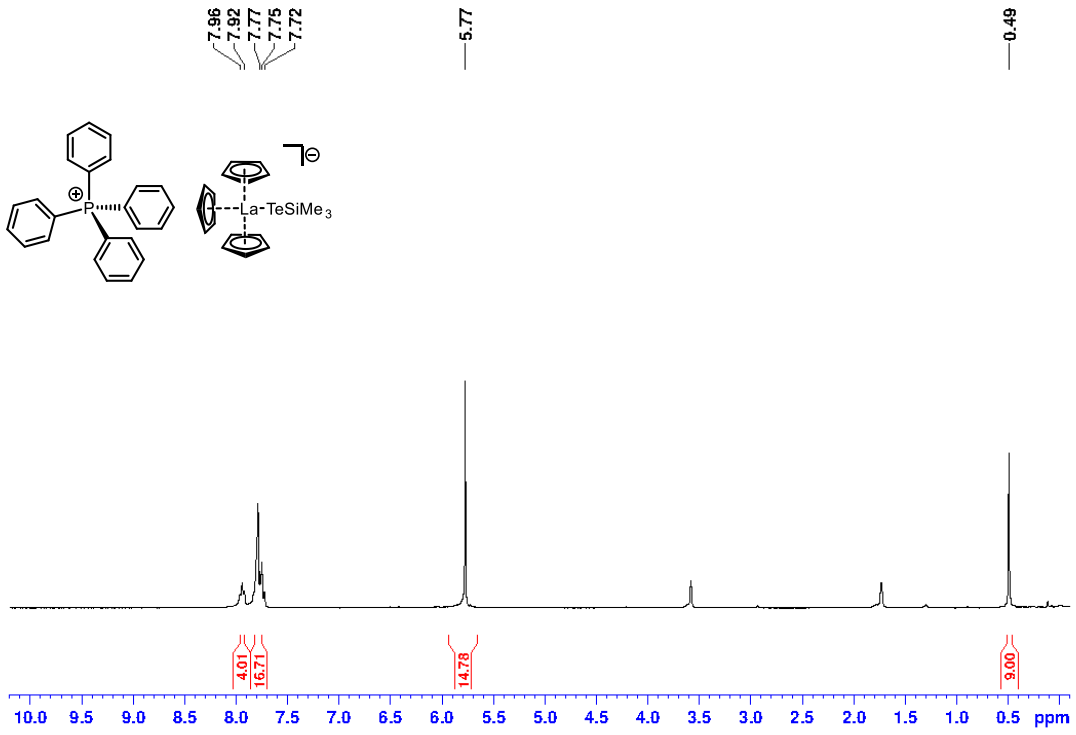

Figure S32. ^{1}H-NMR spectrum (300.25 MHz, thf-d_8) of $PPh_4[Cp_3LaTeSiMe_3]$ (**4-Te**).

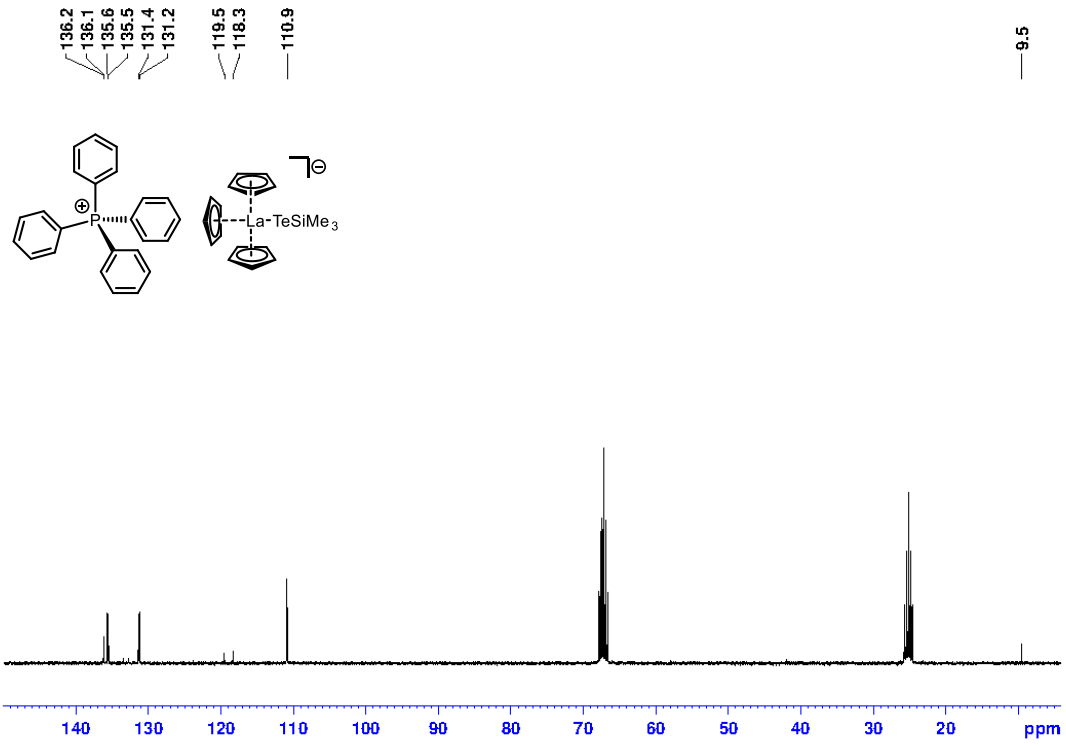

Figure S33. ^{13}C-NMR spectrum (75.5 MHz, thf-d_8) of $PPh_4[Cp_3LaTeSiMe_3]$ (**4-Te**).

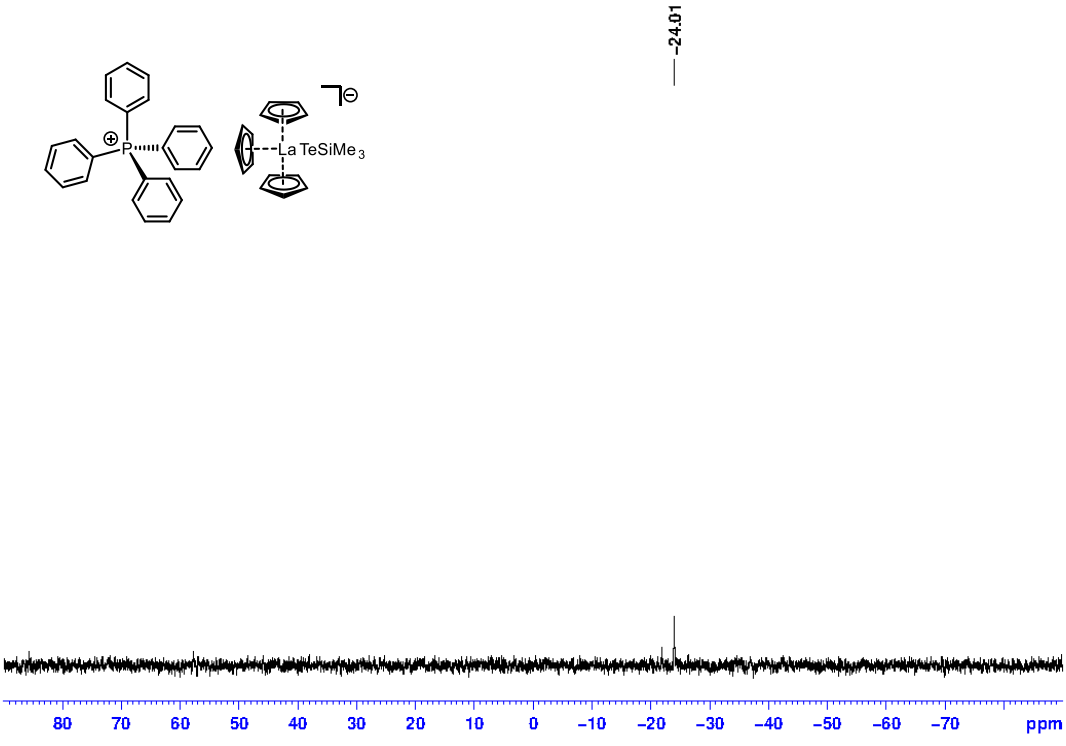

Figure S34. ^{29}Si-NMR spectrum (59.65 MHz, thf-d_8) $PPh_4[Cp_3LaTeSiMe_3]$ (**4-Te**).

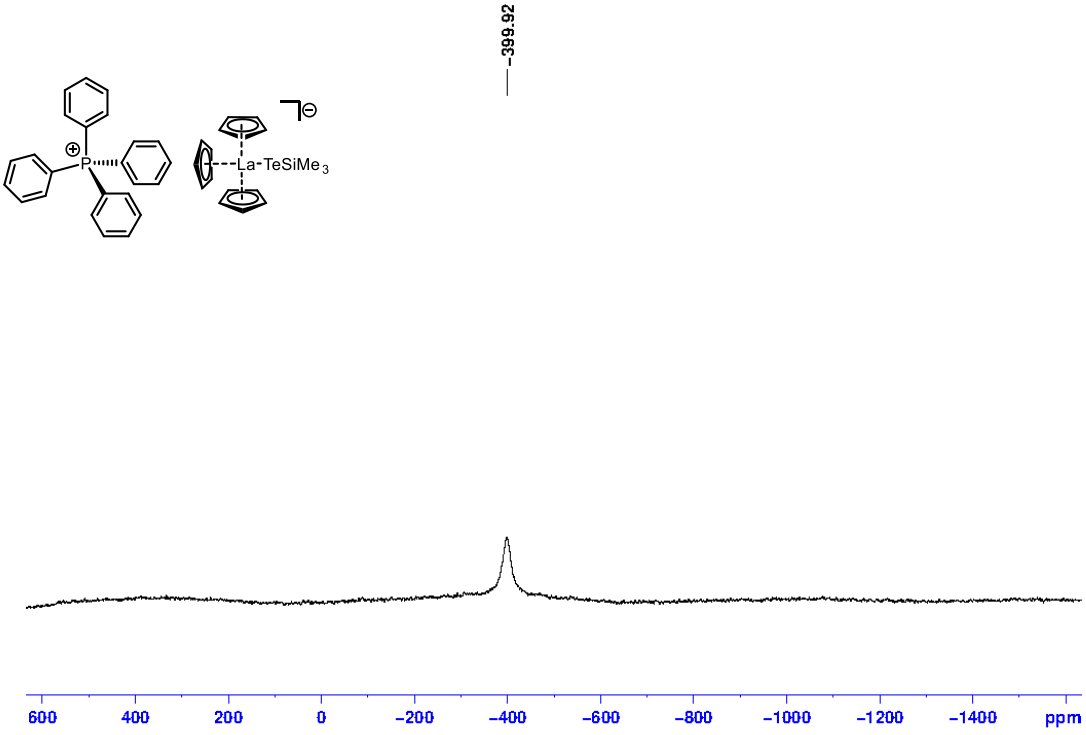

Figure S35. ^{139}La-NMR spectrum (42.41MHz, thf-d_8) $PPh_4[Cp_3LaTeSiMe_3]$ (**4-Te**).

3. Crystallographic data

The data collection for the single-crystal structure determination was performed on a Stoe Stadivari diffractometer (microfocus source, Cu-K_α radiation, Dectris PILATUS 300K detector) or a Bruker D8 Quest diffractometer (microfocus source, Mo-K_α radiation, PHOTON 100 or PHOTON III C14 detector) by the X-ray service department of the Fachbereich Chemie, University of Marburg at 100K. Information concerning the used hardware, and software used for Data collection, cell refinement and data reduction as well as structure solution and refinement can be reviewed in the following CIF-files: CCDC 2087069 PPh_4F (**1**), 2087070 PPh_4[S-TMS] (**3-S**), 2087071 PPh_4[Se-TMS] (**3-Se**), 2087072 PPh_4[Te-TMS] (**3-Te**), 2087073 $(Me_2N)_3P{=}N{=}P(NMe_2)_3[OCO_2Me]$ (**2-PPNMe2**), 2087074 $PPh_4[Cp_3LaS\text{-}TMS]$ (**4-S**), 2087075 $PPh_4[Cp_3LaSe\text{-}TMS]$ (**4-Se**), 2087076 $PPh_4[Cp_3LaTe\text{-}TMS]$ (**4-Te**), and 2087077 $Ph_3P{=}N{=}PPh_3[OCO_2Me]$ x 0.5 MeCN (**2-PPN**). After solution (Shelxt)[5] and refinement process (Shelxl 2018/3)[6,7] the data was validated by using Platon.[8] All non-hydrogen atoms were refined with anisotropic displacement parameters. All hydrogen atoms were placed at calculated positions and included in the refinement using a riding model. All graphic representations were created with Diamond 4.[9] Displacement ellipsoid plots were prepared at 50% probability displacements for non-hydrogen atoms.

Table S1: XRD-data of **1, 2-PPN** and **2-PPNNMe$_2$**

	Ph_4PF (1)	**PPN[$MeCO_3$] · 0.5 MeCN (2-PPN)**	**$PPNMe_2$[$MeCO_3$] (2-$PPNNMe_2$)**
CCDC code	2087069	2087077	2087073
Identification code	tvdpph4floesen	hq07_0m_a_PPNMeCO3	TVD136loesen
Empirical formula	$C_{24}H_{20}FP$	$C_{78}H_{69}N_3O_6P_4$	$C_{14}H_{39}N7O_3P_2$
Formula weight	358.37	1268.24	415.46
Temperature/K	100(2)	100(2)	100(2)
Crystal system	monoclinic	monoclinic	triclinic
Space group	$P2_1/n$	$P2_1/c$	$P\bar{1}$
a/Å	9.7884(4)	10.620(2)	7.9237(2)
b/Å	18.6328(6)	35.750(7)	11.4184(4)
c/Å	10.2715(4)	17.320(3)	12.706(4)
α/°	90	90	103.005(2)
β/°	90.900(3)	97.36(3)	98.958(2)
γ/°	90	90	96.125(2)
Volume/Å^3	1873.14(12)	6521(2)	1094.44(6)
Z	4	4	2
ρ_{calc}g/cm^3	1.271	1.292	1.261
μ/mm^{-1}	1.398	0.174	2.041
F(000)	752	2664	452
Crystal size/mm^3	0.226 × 0.186 × 0.155	0.633 × 0.310 × 0.232	0.264 × 0.178 × 0.133
Radiation	CuKα (λ = 1.54186)	MoKα (λ = 0.71073)	CuKα (λ = 1.54186)
Theta range for data collection/°	4.746 to 66.499	4.42 to 49.998	4.017 to 66.482
Index ranges	$-11 \le h \le 10$, $-11 \le k \le 22$, $-10 \le l \le 12$	$-12 \le h \le 12$, $-42 \le k \le 42$, $-20 \le l \le 20$	$-9 \le h \le 9$, $-10 \le k \le 13$, $-15 \le l \le 15$
Reflections collected	13605	175989	18979
Independent reflections	3299 [R_{int} = 0.0234, R_{sigma} = 0.0170]	11537 [R_{int} = 0.0607]	3829 [R_{int} = 0.0354]
Completeness to θ (x=)	99.8% (x=66.499°)	99.9% (x= 25.000°)	99.4% (x=66.482°)
Absorption correction	Semi-empirical from equivalents	Semi-empirical from equivalents	Semi-empirical from equivalents
Max. and min. transmission	0.8143 and 0.3496	0.7455 and 0.6858	0.5688 and 0.0930
Refinement method	Full-matrix least-squares on F^2	Full-matrix least-squares on F^2	Full-matrix least-squares on F^2
Data/restraints/parameters	3299/0/235	11537/6/823	3829/0/248

Goodness-of-fit on F^2	1.037	1.093	1.030
Final R indexes [I>=2σ (I)]	R_1 = 0.0312, wR_2 = 0.0851	R_1 = 0.0412, wR_2 = 0.0905	R_1 = 0.0478, wR_2 = 0.1314
Final R indexes [all data]	R_1 = 0.0339, wR_2 = 0.0866	R_1 = 0.0544, wR_2 = 0.0961	R_1 = 0.0554, wR_2 = 0.1354
Largest diff. peak/hole / e $Å^{-3}$	0.313/-0.348	0.608/-0.328	0.280/-0.439

Table S2: XRD-data of **3-S, 3-Se, 3-Te**.

	$Ph_4P[SSiMe_3]$ (3-S)	**$Ph_4P[SeSiMe_3]$ (3-Se)**	**$Ph_4P[TeSiMe_3]$ (3-Te)**
CCDC code	2087070	2087071	2087072
Identification code	jg224loesen_Ph4PSSiMe3	af01_0m_a_Ph4PSeSiMe3	jg354loesen_Ph4PTeSiMe3
Empirical formula	$C_{27}H_{29}PSSi$	$C_{27}H_{29}PSeSi$	$C_{27}H_{29}PSiTe$
Formula weight	444.62	491.52	540.16
Temperature/K	100(2)	100(2)	100(2)
Crystal system	orthorhombic	monoclinic	monoclinic
Space group	*Pbca*	$P2_1/c$	$P2_1$
a/Å	17.6627(3)	10.511(2)	9.5283(2)
b/Å	15.3022(3)	9.071(2)	10.6121(2)
c/Å	18.0163(4)	26.773(5)	12.3821(3)
α/°	90	90	90
β/°	90	99.08(3)	90.136(2)
γ/°	90	90	90
Volume/$Å^3$	4869.41(17)	2520.8(9)	1252.02(5)
Z	8	4	2
ρ_{calc}g/cm^3	1.213	1.295	1.433
μ/mm^{-1}	2.344	1.612	10.510
F(000)	1888	1016	544
Crystal size/mm^3	0.231 × 0.187 × 0.151	0.624 × 0.286 × 0.197	0.371 × 0.176 × 0.077
Radiation	CuKα (λ = 1.54186)	MoKα (λ = 0.71073)	CuKα (λ = 1.54186)
Theta range for data collection/°	4.909 to 66.496°	2.296 to 27.124	7.14 to 132.974
Index ranges	$-20 \le h \le 9$, $-18 \le k \le 18$, $-21 \le l \le 21$	$-13 \le h \le 13$, $-11 \le k \le 11$, $-32 \le l \le 34$	$-11 \le h \le 11$, $-12 \le k \le 11$, $-13 \le l \le 14$
Reflections collected	42306	57425	19271
Independent reflections	4276 [R_{int} = 0.0326]	5577 [R_{int} = 0.0480]	3978 [R_{int} = 0.0501]
Completeness to θ (x=)	99.8% (x=66.496°)	100% (x= 25.000°)	
Absorption correction	Semi-empirical from equivalents	Semi-empirical from equivalents	Semi-empirical from equivalents
Max. and min. transmission	0.84333 and 0.3338	0.7455 and 0.6221	
Refinement method	Full-matrix least-squares on F^2	Full-matrix least-squares on F^2	Full-matrix least-squares on F^2
Data/restraints/parameters	4276/0/274	5577/0/274	3978/1/276
Goodness-of-fit on F^2	1.140	1.032	1.062
Final R indexes [I>=2σ (I)]	R_1 = 0.0357, wR_2 = 0.1045	R_1 = 0.0273, wR_2 = 0.0588	R_1 = 0.0415, wR_2 = 0.1103
Final R indexes [all data]	R_1 = 0.0395, wR_2 = 0.1064	R_1 = 0.0345, wR_2 = 0.0615	R_1 = 0.0438, wR_2 = 0.1119
Largest diff. peak/hole / e $Å^{-3}$	0.219/-0.408	0.414/-0.318	1.043/-1.176
Extinction coefficient			0.0020(4)
Absolute structure parameter			0.051(10)

Table S3: XRD-data of **4-S, 4-Se** and **4-Te**.

	$Ph_4P[Cp_3LaSSiMe_3]$ (4-S)	**$Ph_4P[Cp_3LaSeSiMe_3]$ (4-Se)**	**$Ph_4P[Cp_3LaTeSiMe_3]$ (4-Te)**
CCDC code	2087075	2087074	2087076
Identification code	JGHW14_0m_a	JG360loesen	JG359La_0m_a
Empirical formula	$C_{42}H_{44}LaPSSi$	$C_{42}H_{44}LaPSeSi$	$C_{42}H_{44}LaPTeSi$
Formula weight	778.80	825.70	874.34
Temperature/K	100(2)	100(2)	100(2)
Crystal system	monoclinic	monoclinic	monoclinic
Space group	$P2_1/c$	$P2_1/n$	$P2_1$
a/Å	14.343(3)	14.1259(9)	9.803(2)
b/Å	15.499(3)	17.0307(9)	14.101(3)
c/Å	16.998(34)	17.0151(11)	13.880(3)
α/°	90	90.00(3)	90
β/°	100.44(3)	111.185(5)	102.94(3)
γ/°	90	90.00(3)	90
Volume/$Å^3$	3704.3(13)	3816.8(4)	1869.8(7)
Z	4	4	2
$\rho_{calc}g/cm^3$	1.396	1.437	1.553
μ/mm^{-1}	1.313	10.633	2.010
F(000)	1592	1664	1016
Crystal size/mm^3	0.2161 × 0.211 × 0.154	0.192 × 0.146 × 0.078	0.396 × 0.166 × 0.128
Radiation	MoKα (λ = 0.71073)	CuKα (λ = 1.54186)	MoKα (λ = 0.71073)
Theta range for data collection/°	2.161 to 25.753	3.502 to 66.593	2.318 to 25.759
Index ranges	$-17 \le h \le 17, -18 \le k \le 18, -20 \le l \le 20$	$-16 \le h \le 16, -18 \le k \le 20, -20 \le l \le 16$	$-11 \le h \le 11, -17 \le k \le 17, -16 \le l \le 16$
Reflections collected	98887	35700	54711
Independent reflections	7056 [R_{int} = 0.0503]	6749 [R_{int} = 0.0480]	7108 [R_{int} = 0.0320]
Completeness to θ (x=)	100.0% (x=25.000°)	99.9% (x= 66.593°)	99.9% (x=25.000°)
Absorption correction	Semi-empirical from equivalents	Semi-empirical from equivalents	Semi-empirical from equivalents
Max. and min. transmission	0.7453 and 0.6766	0.0036 and 0.0004	0.7453 and 0.6301
Refinement method	Full-matrix least-squares on F^2	Full-matrix least-squares on F^2	Full-matrix least-squares on F^2
Data/restraints/parameters	7056/0/418	6749/0/418	7108/1/418
Goodness-of-fit on F^2	1.063	0.958	1.052
Final R indexes [I>=2σ (I)]	R_1 = 0.0208, wR_2 = 0.0448	R_1 = 0.0328, wR_2 = 0.0807	R_1 = 0.0149, wR_2 = 0.0342
Final R indexes [all data]	R_1 = 0.0273, wR_2 = 0.0466	R_1 = 0.0382, wR_2 = 0.0821	R_1 = 0.0156, wR_2 = 0.0345
Largest diff. peak/hole / e $Å^{-3}$	0.370/-0.428	0.984/-0.561	0.627/-0.457

XRD-Molecular Structures

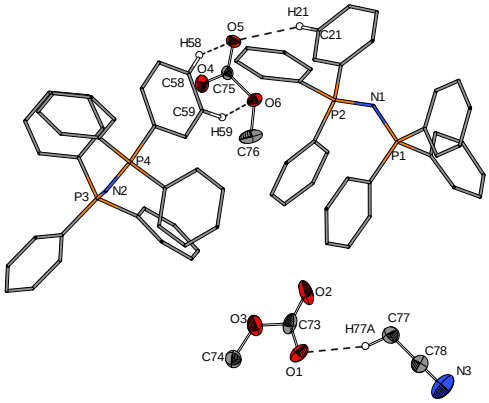

Figure S36. Molecular structure of PPN[OCO_2Me] (**2-PPN**). Ellipsoids of the anions are shown at the 50% level. Only protons involved in some H-Bonds shown for clarity. Selected bond lengths (in Å) and angles (in °): O1-C73 1.244(3), O2-C73 1.238(3), O3-C73 1.415(3), O3-C74 1.410(3), O1-C73-O2 130.8(2), O1-C73-O3 115.4(2), O2-C73-O3 113.8(2), C73-O3-C74 117.0(2), C74-O3-C73-O1 4.0(3), C74-O3-C73-O2 -175.4(2), N3-C78 1.132(3), C78-C77 1.441(4), N3-C78-C77 179.1(3), C77-H77A 0.98, C78-C77-H77A 160.9(2), H77A-O1 2.406(2), C77-H77A-O1 160.9(2), C73-O1-H77A 94.6(2), C73-O1-H77A-C77 32.2(6), O4-C75 1.231(3), O5-C75 1.231(3), O6-C75 1.406(3), O6-C76 1.421(3), O4-C75-O5 130.6(2), O4-C75-O6 116.9(2), O5-C75-O6 112.5(2), C75-O6-C76 116.1(2), C21-H21 0.95, O5-H21 2.50, O5-H21-C21 143.9(1), C75-O5-H21-C21 -81.1(3), C58-H58 0.95, O5-H58 2.34, O5-H58-C58 150.7(1), C75-O5-H58-C58 16.2(3), C59-H59 0.95, O6-H59 2.499(2), C59-H59-O6 140.7(1), C59-H59-O6-C75 -6.6(3).

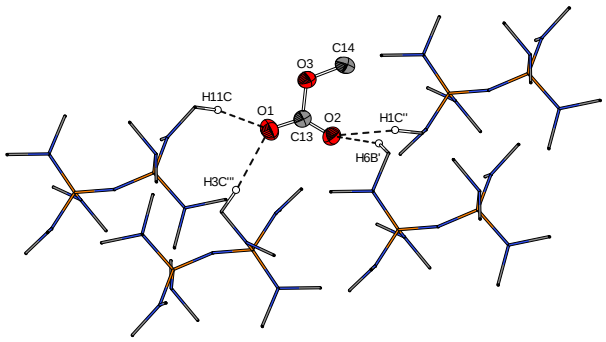

Figure S37. Molecular structure of PPNNMe$_2$[OCO_2Me] (**2-PPNNMe$_2$**). Ellipsoids of the anions are shown at the 50% level. Only protons involved in H-Bonds shown for clarity. Selected bond lengths (in Å) and angles (in °): O3-C14 1.424(3), C13-O3 1.421(3), C13-O1 1.223(3), C13-O2 1.226(3), O2-H1C'' 2.487(2), O2-H6B' 2.481(2), O1-H11C 2.472(2), O1-H3C''' 2.497(2), O1-C13-O2 131.3(2), O2-C13-O3 116.6(2), O1-C13-O3 112.1(2), Symmetry operations: I: x, -1+y, z; II: 1+x, -1+y, z, III: 1-x, 1-y, 1-z.

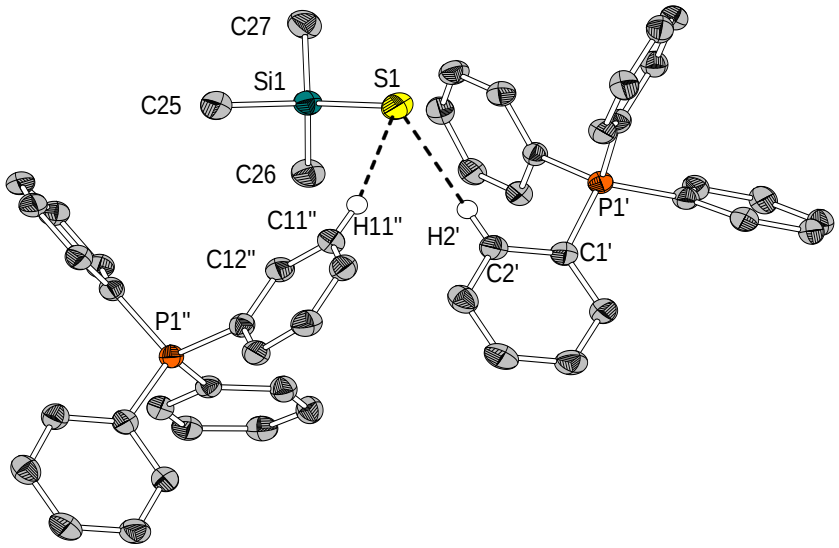

Figure S38. Molecular structure of $Ph_4P[SSiMe_3]$ (**3-S**). Ellipsoids are shown at the 50% level. Only protons involved in H-Bonds shown for clarity. Selected bond lengths (in Å) and angles (in °): S1-Si1 2.0647(8), Si1-C25 1.885(2), Si1-C26 1.885(2), Si1-C27 1.884(2), S1-Si1-C25 115.37(7), S1-Si1-C26 111.30(7), S1-Si1-C27 111.43(7), C25-Si1-C26 106.14(9), C26-Si1-C27 108.7(1), C27-Si1-C25 103.4(1), S1-H2' 2.82, C2'-H2' 0.93, S1-H2'-C2' 143(1), Si1-S1-H2'-C2' -138.9(2), C1'-C2' 1.393(3), C1'-C2'-H2' 120.3(2), C1'-C2'-H2'-S1' -120.2(2), S1-H11'' 2.85, C11''-H11'' 0.93, Si1-S1-H11''-C11'' 22.8(3), C12''-C11'' 1.385(3), C12''-C11''-H11'' 120.2(2), C12''-C11''-H11''-S1 -1.7(4). Symmetry operations: I: 1/2+x, y, 1/2-z; II: 1-x, -1/2+y, 1/2-z.

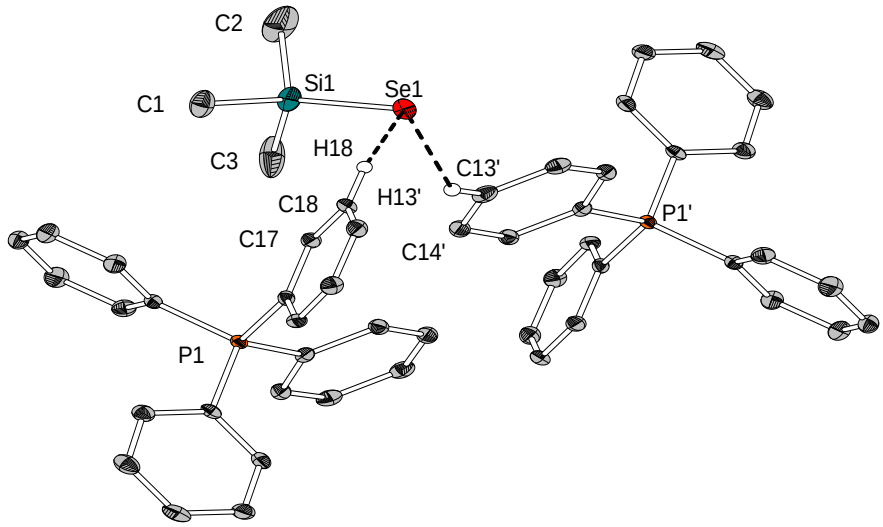

Figure S39. Crystallographically determined molecular structure of $Ph_4P[SeSiMe_3]$ (**3-Se**). Ellipsoids of are shown at the 50% level. Only protons involved in H-Bonds shown for clarity. Selected bond lengths (in Å) and angles (in °): Se1-Si1 2.2102(9), Si1-C1 1.882(2), Si1-C2 1.880(3), Si1-C3 1.880(3), Se1-Si1-C1 113.75(7), Se1-Si1-C2 111.0(1), Se1-Si1-C3 112.9(8), C1-Si1-C2 111.01(1), C2-Si1-C3 108.0(2), C3-Si1-C1 106.0(1), Se1-H13‘ 2.93, C13‘-H13‘ 0.95, Se1-H13‘-C13‘, 144.9(1), Si1-Se1-H13‘-C13‘ 108.6(2), C14‘-C13‘ 1.389(3), C14‘-C13‘-H13‘ 119.9, C14‘-C13‘-H13‘-Se1 -147,5(1), Se1-H18 2.92, Se1-H18-C18 132,4(1), Si1-Se1-H18-C18 70.1(1), C17-C18 1.385(2), C17-C18-H18 120.0, C17-C18-H18-Se1 -21.6(2). Symmetry operations: I: 2-x, 1-y, 1-z.

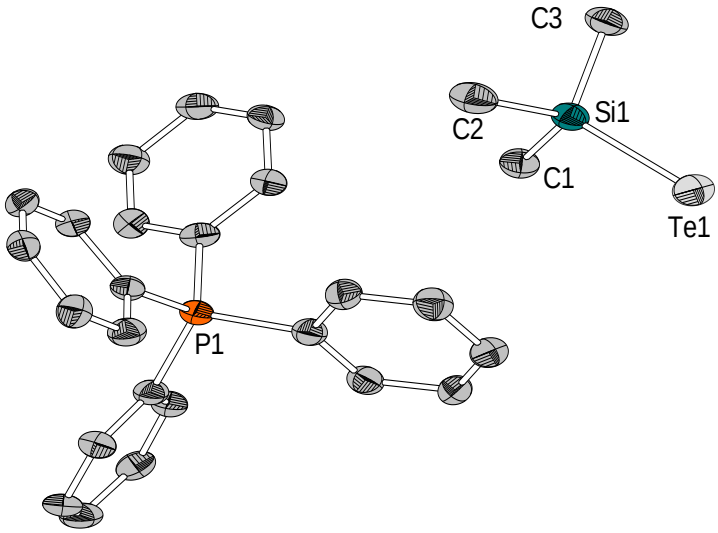

Figure S40. Crystallographically determined molecular structure of Ph_4P [$TeSiMe_3$] (**3-Te**). Ellipsoids are shown at the 50% level. Protons are omitted for clarity. Selected bond lengths (in Å) and angles (in °): Te1-Si1 2.447(2), Si1-C1 1.884(9), Si1-C2 1.89(1), Si1-C3 1.89(1), Te1-Si1-C1 111.7(3), Te1-Si1-C2 113.8(3), Te1-Si1-C3 113.8(3), C1-Si1-C2 106.9(4), C2-Si1-C3 104.5(4), C3-Si1-C1 105.5(4).

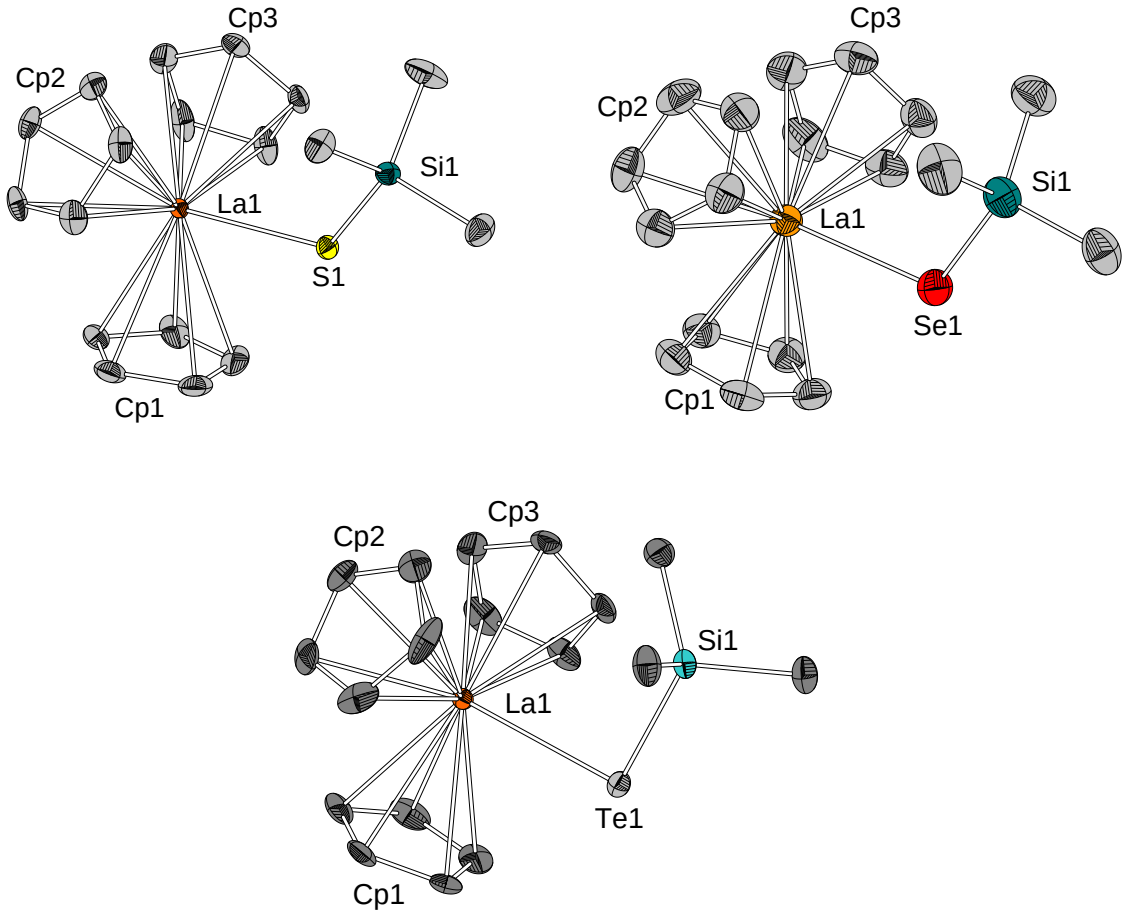

Figure S41. Crystallographically determined molecular structures of Ph_4P [$Cp_3LaSSiMe_3$] (**4-S**) (top row left), Ph_4P [$Cp_3LaSeSiMe_3$] (**4-Se**) (top row right) and Ph_4P [$Cp_3LaTeSiMe_3$] (**4-Te**) (bottom row). The are no bonding interactions within ion pairs. Ellipsoids are shown at the 50% level. The cation and protons are omitted for clarity. Refer to Table S4 for important bond lengths- and angles.

Table S4: Selected bond lengths (in Å) and angles (in °): **4-S** (left row), **4-Se** (middle row) and **4-Te** (right row). As all Cp-rings are connected to La in a η^5-fashion, bond parameters with Cp refer to the $Cp_{centroid}$ position always.

4-S		**4-Se**		**4-Te**	
La1-S1	2.9222(7)	La1-Se1	2.998(6)	La1-Te1	3.283(8)
S1-Si1	2.098(8)	Se1-Si1	2.236(1)	Te1-Si1	2.475(1)
La1-S1-Si1	128.33(3)	La1-Se1-Si1	117.34(4)	La1-Te1-Si1	106.27(3)
S1-La1-Cp3	104.01(2)	Se1-La1-Cp3	104,59(1)	Te1-La1-Cp3	106.86(1)
S1-La1-Cp2	107.27(2)	Se1-La1-Cp2	104.74(1)	Te1-La1-Cp2	101.46(1)
S1-La1-Cp1	94.49(2)	Se1-La1-Cp1	95.54(1)	Te1-La1-Cp1	95.96(1)
La1-Cp3	2.6249(7)	La1-Cp3	2.6075(3)	La1-Cp3	2.5950(6)
La1-Cp2	2.6047(8)	La1-Cp2	2.5951(3)	La1-Cp2	2.5949(8)
La1-Cp1	2.5885(9)	La1-Cp1	2.6137(4)	La1-Cp1	2.5977(6)
Cp3-La1-Cp2	112,93(2)	Cp3-La1-Cp2	116.28(1)	Cp3-La1-Cp2	115.82(1)
Cp2-La1-Cp1	117.54(2)	Cp2-La1-Cp1	116.25(1)	Cp2-La1-Cp1	116.59(1)
Cp1-La1-Cp3	117.17(2)	Cp1-La11-Cp3	115.51(1)	Cp1-La1-Cp3	116.08(1)
Si1-C40	1.868(3)	Si1-C42	1.872(4)	Si1-C42	1.873(4)
Si1-C42	1.874(3)	Si1-C40	1.868(5)	Si1-C41	1.875(4)
Si1-C41	1.879(3)	Si-C41	1.879(5)	Si1-C40	1.877(5)
Si-S-La-Cp1	-170.36(4)	Si1-Se1-La1-Cp1	-174.81(3)	Si1-Te1-La1-Cp1	-175.88(3)
La1-S1-Si1-C41	179.4(1)	La1-Se1-Si1-C41	-170.7(1)	La1-Te1-Si1-C40	-17.5(1)

4. Thermal Analysis Studies

TGA measurements were performed in a glovebox under nitrogen inertgas with a DSC-TGA 3 (Mettler Toledo) for a limited number of samples in order to get a first impression of the decomposition temperatures of certain ionic products. The results are presented in Figure S42 and Figure S43

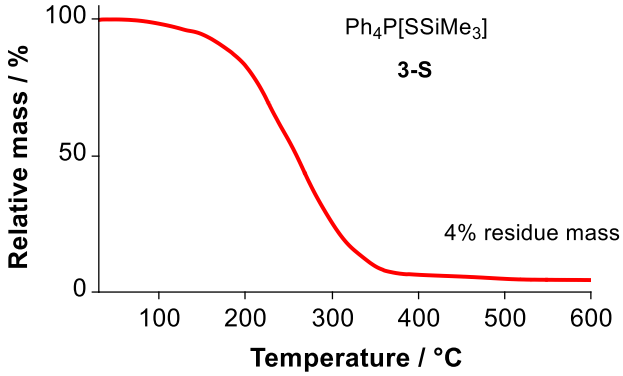

Figure S42: TGA measurement of **3-S** (30°C-600°C, 10 K min^{-1}).

Figure S43 shows the thermogravimetric measurements for **4-S** and **4-Te**.

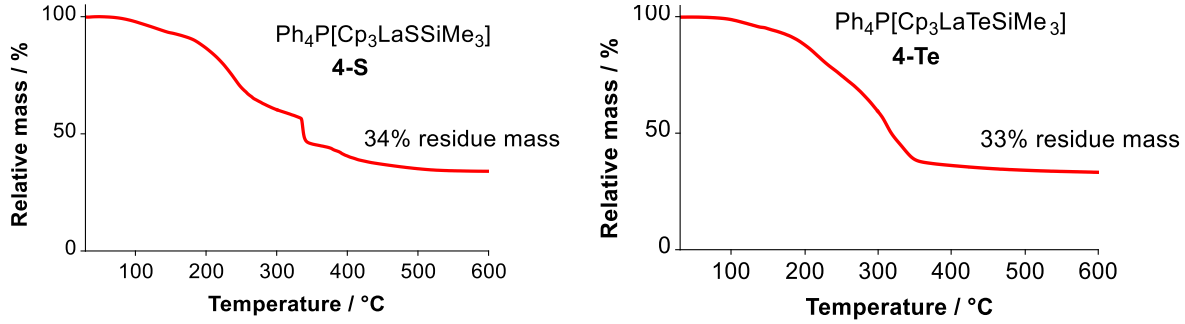

Figure S43. TGA measurements of **4-S** (left) and **4-Te** (right) (30°C-600°C, 10 K min^{-1}).

5. References

1 C. Bolli, J. Gellhaar, C. Jenne, M. Keßler, H. Scherer, H. Seeger and R. Uzun, *Dalton Trans.*, 2014, **43**, 4326–4334.

2 R. Link and R. Schwesinger, *Angew. Chem. Int. Ed.*, 1992, **31**, 850. *Angew. Chem.*, 1992, **104**, 864.

3 R. Schwesinger, R. Link, P. Wenzl and S. Kossek, *Chem. Eur. J.*, 2005, **12**, 438–445.

4 L. H. Finger, J. Guschlbauer, K. Harms and J. Sundermeyer, *Chem. Eur. J.*, 2016, **22**, 16292–16303.

5 G. M. Sheldrick, *Acta Cryst. A*, 2015, **71**, 3–8.

6 C. B. Hübschle, G. M. Sheldrick and B. Dittrich, *J. Appl. Cryst.*, 2011, **44**, 1281–1284.

7 G. M. Sheldrick, *Acta Cryst. C*, 2015, **71**, 3–8.

8 A. L. Spek, *Acta Cryst. D*, 2009, **65**, 148–155.

9 H. P. K. Brandenburg, *Diamond*, Crystal Impact GbR, Bonn, 2012.